Theoretical study of grain boundaries in Si: Effects of structural disorder on the local electronic structure and the origin of band tails

Masanori Kohyama

Department of Material Physics, Osaka National Research Institute, Agency of Industrial Science and Technology, 1-8-31 Midorigaoka, Ikeda, Osaka 563, Japan

Ryoichi Yamamoto

Institute of Industrial Science, University of Tokyo, 7-22-1 Roppongi, Minato-ku, Tokyo 106, Japan
(Received 27 December 1993; revised manuscript received 9 June 1994)

The atomic and electronic structures of the $\{122\}$ $\Sigma=9$ tilt and $\langle 111 \rangle$ $\Sigma=7$ and $\langle 011 \rangle$ $\Sigma=3$ twist boundaries in Si have been examined by using the transferable semiempirical tight-binding method. The effects of various kinds of structural disorder, except coordination defects, on the local electronic structure of Si at the interfaces have been analyzed, and the origins of band tails at grain boundaries in Si have been investigated. Odd-membered rings induce the changes in the shapes of the local densities of states (LDOS's), where the densities of states are increased at the two minima among the three peaks of the bulk valence-band DOS and are decreased at the s-p mixing peak. Four-membered rings generate the LDOS's of a particular shape, where the sharp s-like and p-like peaks are shifted toward the bottom and the top of the valence band, respectively, and the features between these two peaks are smoothed. Bond distortions, strictly bond stretchings and bond-angle distortions, generate states at the top of the valence band and at the bottom of the conduction band, inducing the peaks at the band edges in the LDOS's. Greatly stretched bonds generate so-called weak-bond states, which consist of the bonding and antibonding states inside the minimum band gap. These states are deeper in the band gap and are more spatially localized at the bond and neighboring atoms than the shallow band-edge states caused by smaller bond distortions. Dihedral-angle disorder does not induce such marked changes in the LDOS's, although there exists a slight shift of the p-like peak toward lower energy, which seems to be related to the suppression of bulklike states at the top of the valence band. The present relations between the structural disorder and the local electronic structure of Si also apply to general disordered systems such as amorphous Si. It can be said that the effects of the respective kinds of structural disorder have been shown much more clearly than in the previous studies of amorphous Si because here the respective kinds of disorder can be arranged and buried properly between the bulk crystals in the configurations of grain boundaries. Regarding band tails, it has been shown that the band-edge states caused by bond distortions can penetrate into the minimum band gap according to the degree of bond distortions, and that those in the coincidence-site-lattice (CSL) tilt boundaries do not penetrate into the minimum band gap because of small bond distortions. The band-edge states coming from bond distortions are frequently localized in the interface layers, although these are not necessarily localized in the directions parallel to the interface. Greater bond distortions existing isolated or sparsely in the interface generate states deeper in the band gap with stronger localization behavior in the directions parallel to the interface as in the case of the present weak-bond states. The band tails at grain boundaries in Si observed experimentally can be explained by the distribution of such distorted or weak bonds in general grain boundaries or at defects in the CSL tilt boundaries. This is the first theoretical study that has successfully explained the origins of the band tails at grain boundaries in Si.

I. INTRODUCTION

It is well known that grain boundaries in semiconductors significantly affect the electronic properties of polycrystalline semiconductors used for solar cells or various electronic devices such as thin-film transistors (TFT's), through the generation of shallow or deep states in the band gap, or through interactions with impurities or dopants.[1,2] Thus it is of much importance to investigate the atomic and electronic structures of grain boundaries in semiconductors.

Significant advances have been made in the understanding of the coincidence-site-lattice (CSL) tilt boundaries in elemental semiconductors such as Si or Ge,[2] which frequently exist in polycrystalline samples as majorities.[3] Many HRTEM (high-resolution transmission electron microscopy) observations[2,4-9] have indicated that such CSL tilt boundaries in Si or Ge are constructed by arranging structural units consisting of atomic rings without any coordination defects. Further, many theoretical calculations[10-18] of the atomic and electronic structures of such CSL tilt boundaries have shown that

<u>50</u>   8502

such configurations can exist stably with relatively small bond distortions, and that such configurations contain no electronic states inside the minimum band gap between the bulk valence-band maximum and the bulk conduction-band minimum. This is consistent with experiments indicating that the CSL tilt boundaries in Si or Ge are intrinsically electrically nonactive.[2]

However, there exist many experiments indicating the presence of band tails or midgap states at grain boundaries in Si or Ge.[19−23] Thus it can be considered[2,24,25] that such gap states should be associated with general disordered boundaries containing greater structural disorder than the CSL tilt boundaries, or with defects in the CSL tilt boundaries, or with segregated or precipitated impurities or dopants. Thus, as the next step, it is of much interest to investigate the atomic and electronic structures of grain boundaries in Si or Ge containing greater structural disorder than the CSL tilt boundaries. And it is of much importance to clarify the effects of structural disorder on the local electronic structure at interfaces in order to elucidate the origins of the observed band tails or midgap states at grain boundaries in Si.

As reported in our preceding paper,[26] which is referred to as paper I in the present paper, we have dealt with various kinds of twist boundaries in Si—the $\langle 111 \rangle$ $\Sigma = 7$, $\langle 011 \rangle$ $\Sigma = 3$, and $\langle 001 \rangle$ $\Sigma = 5$ twist boundaries, as well as the $\{122\}$ $\Sigma = 9$ tilt boundary as a typical CSL tilt boundary in Si—theoretically by using the transferable semiempirical tight-binding (SETB) method.[27,28] We have examined energies and atomic configurations of the twist boundaries against various rigid-body translations, and found that the twist boundaries contain much greater structural disorder and much larger interfacial energies than the CSL tilt boundaries in Si, similarly to the *ab initio* calculations of $\langle 001 \rangle$ twist and tilt boundaries in Ge.[29] These results can explain the observed predominance of the CSL tilt boundaries in polycrystalline Si.[3] Further, we have found that various shallow or deep states in the band gap are generated in the twist boundaries in Si, in contrast to the CSL tilt boundaries which contain no states inside the minimum band gap.

In the present paper following paper I, we perform detailed analyses of the atomic and electronic structures of the $\{122\}$ $\Sigma = 9$ tilt boundary and the $\langle 111 \rangle$ $\Sigma = 7$ and $\langle 011 \rangle$ $\Sigma = 3$ twist boundaries with several types of rigid-body translations.[30] The present interfaces of the tilt and twist boundaries contain various kinds of structural disorder, with the exception of coordination defects, such as odd-membered rings, bond-length and bond-angle distortions, dihedral-angle distortions, four-membered rings, and greatly stretched bonds. In this paper, we investigate the effects of such kinds of structural disorder on the local electronic structure of Si at the interfaces. The analyses of the $\langle 001 \rangle$ $\Sigma = 5$ twist boundaries and the coordination defects will be given in our following paper, which is referred to as paper III.

As will be shown in this paper, the present kinds of structural disorder have various effects on the electronic structure of Si, and some kinds of structural disorder at the interfaces can generate boundary-localized states at the band edges penetrating into the minimum band gap.

These can be regarded as candidates for the origins of the experimentally observed band tails at grain boundaries in Si.[19−22] This theoretical study presents realistic models of the origins of the band tails at grain boundaries in Si.

It should be noted that no previous theoretical calculations of grain boundaries in Si successfully explained the origins of the band tails. As mentioned above, the calculated boundary-localized states in the CSL tilt boundaries in Si or Ge (Refs. 11 and 14–18) do not penetrate into the minimum band gap. Also, such states seem not to be localized in directions parallel to the interface, but only in the direction normal to the interface. Thus there remain questions[2,21,31] such as why the CSL tilt boundaries in Si do not contain shallow states inside the minimum band gap, how great is the disorder needed to generate such states penetrating into the minimum band gap manifested as band tails, or what structural disorder generates states well-localized in directions parallel to the interface as well as normal to the interface. In this paper, these questions are answered, and the long-standing discrepancy[2,21,31] between theoretical studies and experiments with band tails at grain boundaries in Si is settled.

The present results of the effects of structural disorder at grain boundaries in Si should also apply to general disordered systems such as amorphous Si. It should be noted that the atomic structures of the present interfaces can be regarded as being composed of local structural units common to amorphous Si. As is well known, it is of great scientific and technological importance to clarify the relations between the local structural disorder and the electronic properties of amorphous Si. The effects of structural disorder, with the exception of coordination defects, have also been investigated in various theoretical studies of amorphous Si.[32−43] However, in recent theoretical calculations using realistic Hamiltonians and realistic atomic configurations of amorphous Si,[38−41] there exists the problem that it is not easy to analyze the effects of respective kinds of structural disorder, because various kinds of disorder are contained complicatedly with very high densities and with very short periods in the supercell configurations. In contrast, we would like to emphasize that respective kinds of structural disorder can be arranged and buried properly between perfect crystals in the configurations of grain boundaries, which makes it possible to clarify the effects of respective kinds of structural disorder on the bulk electronic structure of Si.

This paper is organized as follows. In Sec. II, the theoretical method and computational scheme are described. In Sec. III, the atomic and electronic structures of the $\{122\}$ $\Sigma = 9$ tilt boundary in Si, and those of the $\langle 111 \rangle$ $\Sigma = 7$ and $\langle 011 \rangle$ $\Sigma = 3$ twist boundaries in Si, are analyzed in detail. Also, the effects of various kinds of structural disorder on the local electronic structure of Si at the interfaces are examined in fine detail. In Sec. IV, relations between the structural disorder and the electronic structure of Si are discussed as compared with the previous theoretical results in amorphous Si. The nature of boundary-localized states is also discussed, and is compared with the localized states in amorphous Si. Finally, the origins of the experimentally observed band tails at grain boundaries in Si are clarified.

II. METHOD OF CALCULATIONS

The atomic and electronic structures of the tilt and twist boundaries in Si have been obtained by energy-minimization calculations using the transferable SETB method[27,28] coupled with the supercell technique. The details of the theoretical method and supercell configurations were given in paper I. Thus we give only a brief overview in this section.

The transferable SETB method was developed in order to overcome the poor transferability of the usual SETB method[44] for structures of Si other than fourfold-coordinated ones. In this method, the binding energy is expressed as a sum of the band-structure energy E_{bs} and the remaining repulsive energy E_{rep}. E_{bs} is obtained by the tight-binding band-structure calculation with the valence atomic-orbital basis, and E_{rep} is given as a sum of short-range interatomic repulsive potentials, similarly to the usual SETB method. However, in the present method, the behavior of the two-center integrals in the Hamiltonian and that of the repulsive potential are modified for large distances, and these are smoothly truncated by attenuation functions. Also, the dependence on the local environment is incorporated into E_{rep} through the effective coordination numbers. Thus the present method well reproduces the energies and equilibrium volumes of variously coordinated structures of Si including a threefold-coordinated one,[26] and deals more correctly with greatly distorted systems of Si. This method also well reproduces the electronic structure, although the bulk band-gap width of Si is overestimated as 2.2 eV. It should be noted that the present Hamiltonian includes second-neighbor interactions in bulk Si. For self-consistency, an on-site electron repulsion term is included through the form of a Hubbard-like Hamiltonian with the value of U used in Ref. 45.

All calculations of the present CSL boundaries are carried out with use of the supercell technique, where a periodicity normal to the interface is imposed by stacking symmetric boundary planes alternately in addition to the two-dimensional periodicity parallel to the interface. Integration over the Brillouin zone is performed by using the special k points.[46]

Lattice relaxations are performed in order to obtain stable configurations, where atomic positions are relaxed according to atomic forces given by the present method. In each step of the relaxations, atomic forces are obtained after the self-consistent iteration, which is terminated if the differences between the input and output occupancies are all kept within 10^{-4} electrons. The relaxation is terminated if all the atomic forces are smaller than 0.1 eV/Å.

In the present paper, we deal with the $\{122\}$ $\Sigma=9$ tilt boundary and the $\langle 111 \rangle$ $\Sigma=7$ and $\langle 011 \rangle$ $\Sigma=3$ twist boundaries in Si. The $\{122\}$ $\Sigma=9$ tilt boundary is constructed by rotating the two crystals around the $\langle 011 \rangle$ axis by 38.9° and the boundary plane (122) is parallel to the rotation axis. The CSL unit cell on the boundary plane is expressed by $R_1=a_0[4,1,-1]/2$ and $R_2=a_0[011]/2$. The supercell contains 144 atoms, where the interfaces are repeated between 72 (122) atomic

layers, and the distance between the interfaces is about 32.6 Å. In the lattice relaxation, all the atoms in the supercell are relaxed.

The present $\langle 111 \rangle$ $\Sigma=7$ twist boundary is constructed by rotating the two crystals around the $\langle 111 \rangle$ axis by 38.2°, and the boundary plane (111) is perpendicular to the rotation axis. The CSL unit cell on the boundary plane is expressed by $R_1=a_0[-3,2,1]/2$ and $R_2=a_0[1,-3,2]/2$. The supercell of this boundary contains 168 atoms, where the interfaces are repeated between 12 (111) layers, and the distance between the interfaces is about 18.8 Å. In the lattice relaxation, the atoms on the central two (111) layers in the bulk regions of the supercell are fixed at the initial positions.

The present $\langle 011 \rangle$ $\Sigma=3$ twist boundary is constructed by rotating the two crystals around the $\langle 011 \rangle$ axis by 109.5°, and the boundary plane (011) is perpendicular to the rotation axis. The CSL unit cell on the boundary plane is expressed by $R_1=a_0[-1,-1,1]$ and $R_2=a_0[2,-1,1]/2$. The supercell contains 156 atoms, where the interfaces are repeated between 13 (011) layers, and the distance between the interfaces is about 25.0 Å. In the lattice relaxation, the atoms on the central (011) layers in the bulk regions of the supercell are fixed at the initial positions.

Rigid-body translations are introduced between the two bulk crystals before the relaxations. In paper I, we examined the energies and atomic configurations of the $\Sigma=7$ and $\Sigma=3$ twist boundaries against various rigid-body translations parallel to the interface within the irreducible parts of the displacement-shift-complete (DSC) unit cells by using the smaller supercells. In this paper, we deal with configurations of the $\Sigma=7$ and $\Sigma=3$ twist boundaries with selected translations parallel to the interface. The definitions of the translations were given in paper I. Translations normal to the interface are set to their optimal values from the smaller supercell calculations. For the $\Sigma=9$ tilt boundary, we also take the optimal normal displacement from the smaller supercell calculations. And we take the translation parallel to the interface for the structure with a glide-plane symmetry from HRTEM observations.[4,6,7,9]

The local densities of states (LDOS's) of relaxed configurations are sampled on k-point meshes with densities larger than that corresponding to the 2048-point uniform mesh in the Brillouin zone of the primitive cell of bulk Si. These are broadened by Gaussians of the form $\exp[-E^2/(2\sigma^2)]$ with $\sigma=0.20$ eV.

III. STRUCTURAL DISORDER AND ELECTRONIC STRUCTURE

A. The $\{122\}$ $\Sigma=9$ tilt boundary: odd-membered rings

Figure 1 shows the relaxed configuration of the $\{122\}$ $\Sigma=9$ tilt boundary in Si. The interface consists of five-membered rings such as $cda'b'e'$ and seven-membered rings such as $abghdcf$. This configuration contains a glide-plane symmetry, and symmetrically equivalent atoms are indicated as a and a', for example, in Fig. 1.
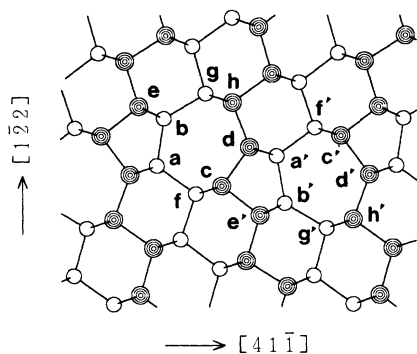
FIG. 1. Relaxed atomic configuration of the {122} $\Sigma=9$ tilt boundary in Si with the rotation angle 38.9°. Atomic positions are projected along the $\langle 011 \rangle$ axis, and open and closed circles indicate the atoms with the two kinds of heights along the $\langle 011 \rangle$ axis. Two sets of five- and seven-membered rings constitute one period along the $\langle 411 \rangle$ direction.

The optimized translation normal to the interface is $+0.06$ Å. The interfacial energy E_{gb} is 0.32 J/m^2. The bond-length and bond-angle distortions range from -1.6% to $+1.5\%$, and from $-16.2°$ to $+20.8°$, respectively. Bond-angle distortions of which the absolute values are larger than 10° are all associated with the odd-(five- and seven-) membered rings. Distortions of $-16.2°$ exist at atoms c and c' of the five-membered rings, and distortions of $+20.8°$ exist at atoms b and b' of the seven-membered rings in Fig. 1. Bond-length distortions of which the absolute values are larger than 1% are also associated with the odd-membered rings and back bonds of the odd-membered rings. Distortions of -1.6% and $+1.5\%$ are associated with the back bonds of the atoms e and e' and g and g' in Fig. 1, respectively.

The present results regarding the energy and the bond distortions are in good agreement with previous calculations of this boundary[10,11,16] and other CSL tilt boun-

daries[13-15,17,18] in Si or Ge. As shown in paper I, the energy and bond distortions of this configuration are much smaller than those for twist boundaries in Si, which is consistent with the observed predominance of this boundary as well as other CSL tilt boundaries in polycrystalline Si.[3]

Figure 2 shows the calculated band structure of this configuration. Boundary-localized states are also plotted. Of course, the boundary-localized states cannot strictly be identified in the supercell calculation. However, it is possible to deduce them from the distribution of wave functions to the interface layers, as is done in the present paper. As shown in Fig. 2, it is clear that there exist no electronic states inside the minimum band gap between the valence-band maximum and the conduction-band minimum, although the boundary-localized states are generated, for example, at the lower edge of the conduction band and at the pseudogaps within the valence band. These results are also in good agreement with previous theoretical results for the same boundary and other CSL tilt boundaries in Si or Ge.[10-18]

The main structural disorder of the present configuration is the odd-membered rings and the associated bond-length and bond-angle distortions. Of course, the effects of these two kinds of disorder cannot clearly be distinguished because odd-membered rings inevitably include some bond distortions. However, the effects of the bond distortions themselves can be analyzed in the configurations without any odd-membered rings, and are mainly concerned with the generation of states at the band edges, as will be shown in Sec. III B. It can be said that the bond distortions and band-edge states of the present configuration are not so remarkable compared with those in other boundaries in following subsections. Thus the main structural disorder of the present configuration can be considered to be the topological disorder of the odd-membered rings.

The effects of odd-membered rings are clear in the LDOS's associated with odd-membered rings. Figure 3 shows LDOS's of interface atoms, and it should be noted
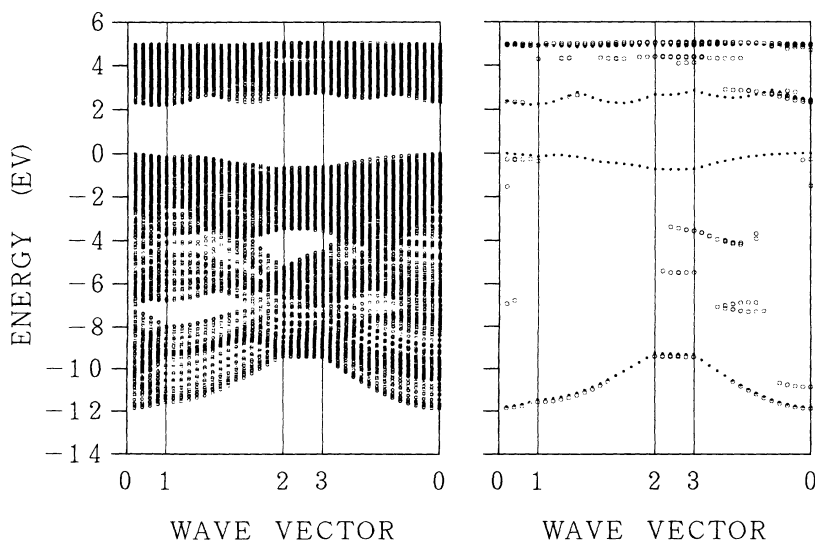
FIG. 2. Band structure and boundary-localized states of the {122} $\Sigma=9$ tilt boundary in Si. In the left panel, all the eigenstates of the supercell are plotted along the lines in the two-dimensional Brillouin zone. In the right panel, the states for which the probability that an electron is located on the atoms of the odd-membered rings at the interface exceeds 60% are plotted. The dotted curves indicate the projected band edges of the perfect crystal. Points 0, 1, 2, and 3 correspond to (0, 0, 0), $(\pi/|\mathbf{R}_1|,0,0)$, $(\pi/|\mathbf{R}_1|,\pi/|\mathbf{R}_2|,0)$, and $(0,\pi/|\mathbf{R}_2|,0)$ in the Brillouin zone of the supercell, where $|\mathbf{R}_1|=3\sqrt{2}a_0/2$ and $|\mathbf{R}_2|=\sqrt{2}a_0/2$.

that symmetrically equivalent atoms have the same LDOS's. As shown in the LDOS's of atoms a, b, c, and d in Fig. 3, remarkable changes of the LDOS's exist at atoms belonging to both the five- and seven-membered rings. As compared with the bulk density of states (DOS), there exist increases at the two valleys among the three peaks of the bulk valence-band DOS, namely the s-like peak, the s-p mixing peak, and the p-like peak. There is also a decrease in the s-p mixing peak.

It should be noted that changes of the present kind are observed even in atoms associated with relatively small bond distortions (atom a), as well as in atoms containing relatively large bond distortions (atoms b and c). This suggests that the present kind of changes in LDOS's are not directly caused by the bond distortions, but mainly by odd-membered rings. The present kind of changes are less marked in LDOS's of atoms belonging either to five-membered rings only or to seven-membered rings only (atoms e, f, g, and h). Thus it seems that the present changes are concerned with intermediate-range order.

The present changes in LDOS's are consistent with the boundary-localized states shown in Fig. 2. The boundary-localized states are generated at about -4 and -7 eV at the pseudogaps within the bulk valence band. We have analyzed the distributions of wave functions of these localized states, and found that the interface atoms such as a, a', b, b', c, c', d, and d' belonging to both the five- and seven-membered rings indeed contain large portions of the respective states. This corresponds to the increases in LDOS's at the two valleys in the valence-band DOS.

Similar changes in LDOS's of the interface atoms have also been found in the calculation of the $\{210\}$ $\Sigma = 5$ tilt boundary in Si (Ref. 17) with the linear muffin-tin orbital (LMTO) method, where the observed changes at the two valleys and the s-p mixing peak may also be attributed to the effects of odd-membered rings, although odd-membered rings were not analyzed in that calculation. Boundary-localized states at the pseudogaps in the valence band have also been observed in previous calcula-
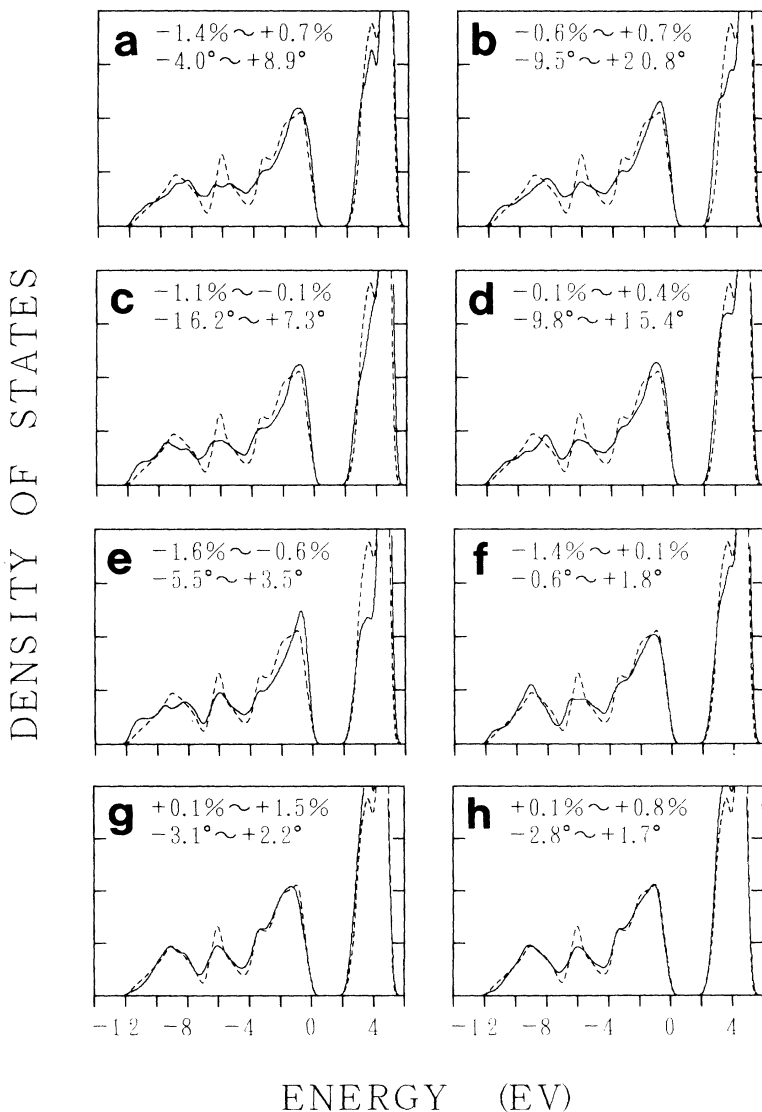
FIG. 3. Local densities of states (LDOS's) of the interface atoms in the $\{122\}$ $\Sigma = 9$ tilt boundary in Si. LDOS's of the atoms labeled in Fig. 1 are shown. The dashed lines indicate the bulk density of states, which is obtained by the LDOS of the central atom in the supercell. The ranges of the bond-length and bond-angle distortions associated with the respective atoms are also shown.

DENSITY OF STATES

ENERGY (EV)

tions of the same boundary[10,16] and other CSL tilt boundaries[14,15,17] in Si.

On the other hand, in the LDOS's of several interface atoms in Fig. 2, there exist slight shifts of the p-like peak toward the valence-band edge, which steepen the shapes of the LDOS's at the band edge. These small changes might also be associated with the odd-membered rings. However, these changes seem to be related more to associated bond distortions than to topological effects, because there seems to be no clear correlation with changes at the two valleys and the s-p mixing peak, and because the effects of bond distortions are mainly the generation of states at the band edges, as will be shown in Sec. III B.

Finally, the boundary-localized states at the lower edge of the conduction band in Fig. 2 also seem to be caused mainly by bond distortions. In the analyses of the distributions of the boundary-localized states of 2.3 and 2.4 eV at point 0 in Fig. 2, we have found that large portions of such respective states exist among the atoms b, b', c, c', d, d', e, and e' in Fig. 1. There exists the tendency that the atoms associated with large bond-angle distortions contain large portions of such states. However, it should be noted that the present conduction-band-edge states do not exist inside the minimum band gap because the bond distortions are relatively small, and that these states are not localized in directions parallel to the interface.

B. The $\langle 111 \rangle$ $\Sigma=7$ twist boundary: bond-length and bond-angle distortions and dihedral-angle distortions

Figure 4 shows the relaxed configuration of the $\langle 111 \rangle$ $\Sigma=7$ twist boundary in Si with the rotation angle 38.2°. The translation parallel to the interface is zero (Trans. 1 in paper I), and the optimized translation normal to the interface is $+0.1$ Å. E_{gb} is 1.28 J/m^2. There exist no coordination defects. The bond-length and bond-angle distortions range from -1.4% to $+4.6\%$ and from
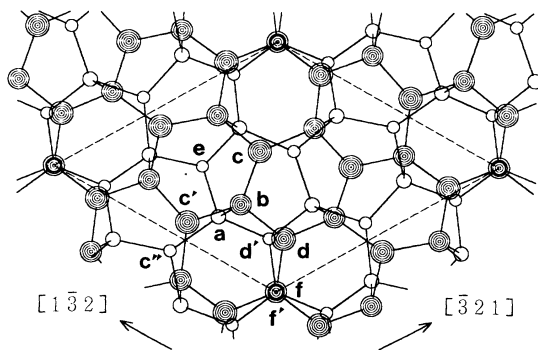
FIG. 4. Relaxed atomic configuration of the $\langle 111 \rangle$ $\Sigma=7$ twist boundary in Si with the rotation angle 38.2°. Atomic positions of the four (111) atomic layers are projected along the $\langle 111 \rangle$ axis, and open and closed circles indicate the atoms of the lower and upper crystals, respectively. The dashed lines indicate the CSL unit cell.

$-23.5°$ to $+21.3°$, respectively. This configuration is the most stable one found in our calculations of the $\langle 111 \rangle$ $\Sigma=7$ boundary with respect to various rigid-body translations in paper I. However, it is clear that the absolute values and density of the bond distortions and E_{gb} are larger than those of the CSL tilt boundaries as discussed in paper I.

As shown in Fig. 4, there exist seven interfacial bonds in the CSL unit cell. One kind of interfacial bond at the coincidence site, namely bond ff', contains only small bond distortions, because this bond is parallel to the rotation axis. The bond-length and bond-angle distortions associated with atoms f and f' range from -1.3 to -0.7% and from $-1.6°$ to $+1.5°$, respectively. However, this bond contains a large dihedral-angle distortion of the rotation angle 38.2° as compared with the staggered configuration in the bulk crystal.

The other six interfacial bonds are all equivalent by the symmetric property of this configuration. Large bond distortions are associated with these interfacial bonds and the back bonds. In Fig. 4, one set of this kind of interfacial bond and neighboring atoms are labeled $a-e$, where symmetrically equivalent atoms are indicated as c, c', and c'', for example. The bond ab is stretched by $+4.5\%$, and the back bonds ac'' and bc are stretched by $+4.6$ and $+3.5\%$, respectively. The bond-angle distortions associated with atoms a and b range from $-14.0°$ to $+21.3°$ and from $-23.5°$ to $+16.8°$, respectively.

It should be noted that this configuration contains no odd-membered rings, but only six-membered rings at the interface, similarly to the bulk regions. Thus this configuration is very effective in order to clarify the effects of bond distortions and the effects of dihedral-angle disorder by excluding the effects of topological disorder such as odd-membered or four-membered rings.

Figure 5 shows the band structure and boundary-localized states of this configuration. It is clear that there exist boundary-localized states at the upper edge of the valence band and the lower edge of the conduction band. In particular, the states at the conduction-band edge exist inside the minimum band gap below the conduction-band minimum by about 0.1 eV, which is in contrast to those of the {122} $\Sigma=9$ tilt boundary and other CSL tilt boundaries in Si.

Figure 6 shows LDOS's of interface atoms. It should be noted that symmetrically equivalent atoms have the same LDOS's. As shown in the LDOS's of atoms a and b at the distorted interfacial bond, it seems that the effects of bond distortions are the generation of peaks in the LDOS's at the top of the valence band and at the bottom of the conduction band. In other words, the effects of bond distortions seems to be the generation of states at the top of the valence band and the bottom of the conduction band. Such states should be the boundary-localized states shown in Fig. 5, especially when they exist in the forbidden energy regions of the bulk crystal.

In the LDOS of the back atom c shown in Fig. 6, peaks at the band edges are also generated. This may be related to the large bond stretchings of $+3.5$ and $+4.6\%$ associated with this atom, and thus the band-edge states are also distributed at this kind of atom. However, as shown
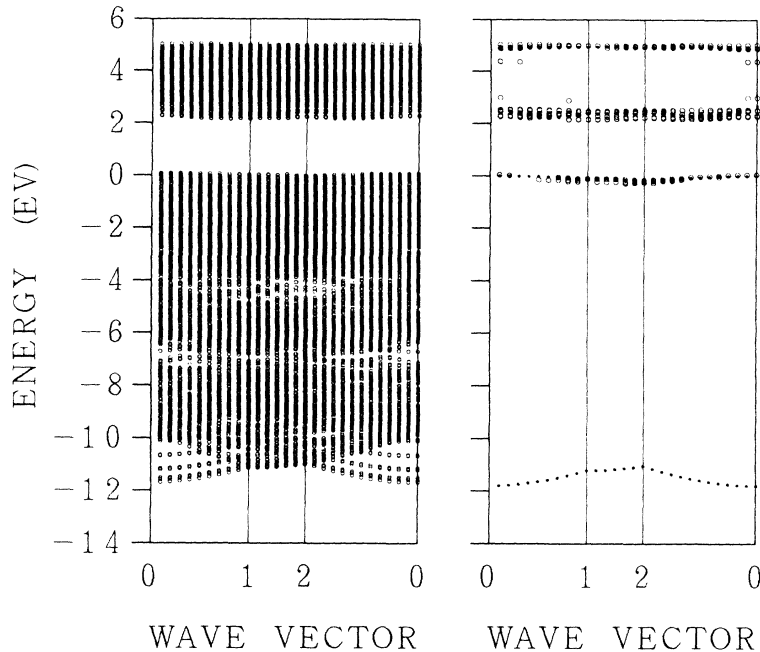
FIG. 5. Band structure and boundary-localized states of the $\langle 111 \rangle$ $\Sigma = 7$ twist boundary in Si. In the left panel, all the eigenstates of the supercell are plotted along the lines in the two-dimensional Brillouin zone. In the right panel, the states for which the probability that an electron is located on the atoms of the four (111) atomic layers at the interface exceeds 70% are plotted. The dotted curves indicate the projected band edges of the perfect crystal. Points 0, 1, and 2 correspond to (0, 0, 0), $(\pi/R_x,0,0)$ and $(\pi/R_x,\pi/(3 \text{ Ry}),0)$ in the Brillouin zone of the supercell, where $R_x = \sqrt{42}a_0/4$ and $R_y = \sqrt{14}a_0/4$.

in Fig. 6, LDOS's of other atoms of the second layers and of the atoms f and f' without large bond distortions do not reveal such large changes, although small increases at the band edges are observed.

It should be noted that no LDOS's reveal remarkable changes similar to those observed in the $\{122\}$ $\Sigma = 9$ boundary as the effects of odd-membered rings. There exist no marked changes in the middle or lower regions of the valence band in the LDOS's in the present configuration containing no odd-membered rings. This clearly indicates that the changes observed in the $\{122\}$ $\Sigma = 9$ boundary are not the effects of bond distortions, but are indeed caused by odd-membered rings as topological disorder.

We have analyzed the distribution of the boundary-localized states in Fig. 5, and obtained the results consistent with the features of the LDOS's. Large portions of the respective valence-band-edge states exist among
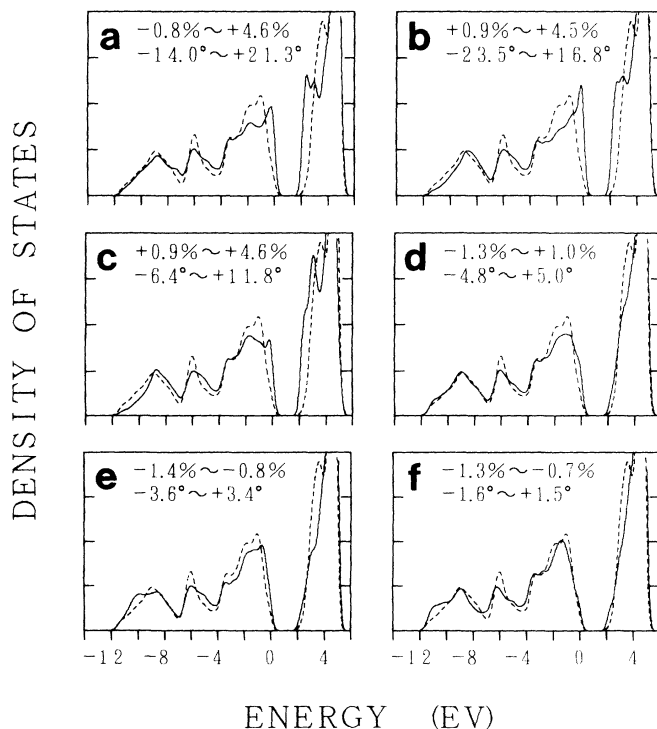
FIG. 6. LDOS's of the interface atoms in the $\langle 111 \rangle$ $\Sigma = 7$ twist boundary in Si. LDOS's of the atoms labeled in Fig. 4 are shown. The dashed lines indicate the bulk density of states, which is obtained by the LDOS of the central atom in the supercell. The ranges of the bond-length and bond-angle distortions associated with the respective atoms are also shown.

atoms b, a, and c, and symmetrically equivalent atoms. For example, about one of the valence-band-edge states of -0.11 eV at point 1 in Fig. 5, the total probability for atom b and equivalent atoms (a total of six atoms) is 25.3%, that for atom a and equivalent atoms is 14.8%, and that for atom c and equivalent atoms is 16.8%. About one of the valence-band-edge states of 0.04 eV at point 0 in Fig. 5, the total probability for atom b and equivalent atoms is 21.5%, that for atom a and equivalent atoms is 14.5%, and that for atom c and equivalent atoms is 13.8%. These results are consistent with the most marked peak at the valence-band edge in the LDOS of atom b in Fig. 6.

Similarly, large portions of the respective conduction-band-edge states exist among atoms a, b, and c, and symmetrically equivalent atoms. For example, about one of the conduction-band-edge states of 2.15 eV at point 1 in Fig. 5, the total probability for atom a and equivalent atoms is 31.0%, that for atom b and equivalent atoms is 17.7%, and that for atom c and equivalent atoms is 19.0%. About one of the conduction-band-edge states of 2.27 eV at point 0 in Fig. 5, the total probability for atom a and equivalent atoms is 39.1%, that for atom b and equivalent atoms is 20.2%, and that for atom c and equivalent atoms is 13.4%. These results are consistent with the most marked peak at the conduction-band edge in the LDOS of atom a in Fig. 6.

In this way, it can be concluded that the effects of bond distortions are the generation of electronic states at the top of the valence band and the bottom of the conduction band, which result in the generation of the peaks in the LDOS's and the generation of the boundary-localized states. Strictly, the present effects should be regarded as those of bond stretchings and bond-angle distortions, because the present configuration contains many stretched bonds as well as bond-angle distortions, and contains only a few contracted bonds.

It seems that the greater the bond distortions, the more deeply the resulting electronic states lie inside the band gap. In the procedure of lattice relaxation, we have found that the position of the uppermost valence-band-edge state gradually approaches from a relatively deep value in the band gap to the present value of 0.05 eV, in accordance with the relaxation of bond distortions. It can be said that relatively small bond distortions generate only band-edge states below the valence-band maximum or above the conduction-band minimum in the cases of the CSL tilt boundaries shown in Sec. III A. Relatively large bond distortions should generate shallow states inside the minimum band gap as in the present case. As will be shown in Sec. III D, greatly distorted bonds generate much deeper weak-bond states inside the minimum band gap.

However, as found in the analysis of the distributions, the present boundary-localized states at the band edges do not reveal a great degree of localization in directions parallel to the interface. The present boundary-localized states are not sharply localized to specific atoms at the interface. These states are localized within the interface layers only in the sense that the wave functions are not propagated into the bulk regions in the direction normal to the interface. For example, about the boundary-localized states at points 1 and 0 in Fig. 5, the distribution of the probability for each atom (not for the total six symmetric atoms) in the CSL unit cell does not exceed 10%, and the respective states are distributed among several interfacial bonds and back atoms in the CSL unit cell. We think that this feature is caused by the high density of the bond distortions in a similar range at the interface, as well as by the effects of the symmetry and two-dimensional periodicity.

Of course, no states are strictly localized in the directions parallel to the interface in the cases of CSL boundaries with two-dimensional periodicity. However, the CSL unit cells on the boundary planes of the present twist boundaries are not so small, and it is possible to analyze the tendency or degree of localization in the directions parallel to the interface by the distribution of wave functions in a similar way to how we measure the degree of localization in the direction normal to the interface in the supercell configurations.

Finally, the changes in the LDOS are not so remarkable in the case of the 38.2° dihedral-angle disorder at the bond ff' as compared with the other interface atoms as shown in Fig. 6. Interactions beyond second neighbors are included in the present Hamiltonian, and no other significant structural disorder is associated with the bond ff'. Thus, it can be said that the effects of dihedral-angle distortion are not so significant. However, in the LDOS of the atom f in Fig. 6, there exist a peculiar slight shift of the p-like peak toward lower energy in contrast to the shifts of this peak toward higher energy observed in the other LDOS's. It is probable that this slight shift of the p-like peak is caused by the suppression of bulk-like states at the top of the valence band by the dihedral-angle disorder as pointed out in Refs. 36 and 37. This point will be discussed in Sec. IV.

C. The $\langle 011 \rangle$ $\Sigma = 3$ twist boundary: four-membered rings

About the $\langle 011 \rangle$ $\Sigma = 3$ twist boundary, we have examined two types of configurations with different translations parallel to the interface. Figure 7 shows the relaxed configuration of this boundary with no translation parallel to the interface (Trans. 1 in paper I), and with the optimized translation normal to the interface of $+0.1$ Å. E_{gb} is 1.02 J/m². This is the most stable configuration found in our calculations of the $\langle 011 \rangle$ $\Sigma = 3$ twist boundary with respect to various rigid-body translations in paper I. However, it is clear that the bond distortions and E_{gb} are larger than those of the CSL tilt boundaries, as discussed in paper I.

This configuration contains no coordination defects. However, there exist two four-membered rings in the CSL unit cell as indicated by arrows in Fig. 7. The CSL unit cell contains three atomic chains along the $\langle 211 \rangle$ direction, as denoted by A, B, and C in Fig. 7. In chains A and C, four-membered rings such as $aba'b'$ and eight-membered rings are repeated alternately, and chain B contains only six-membered rings. Between chains A and B, and B and C, there exist five-membered rings such as
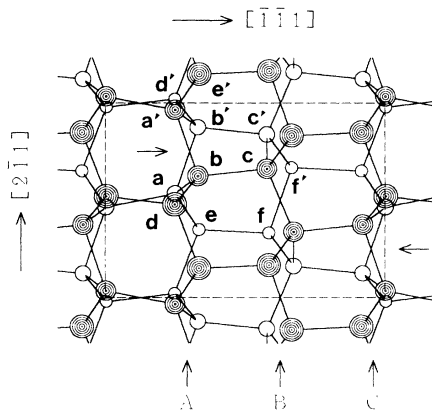
FIG. 7. Relaxed atomic configuration of the ⟨011⟩ Σ=3 twist boundary in Si with the rotation angle 109.5° and Trans. 1. Atomic positions of the four (011) atomic layers are projected along the ⟨011⟩ axis, and open and closed circles indicate the atoms of the lower and upper crystals, respectively. The dashed lines indicate the CSL unit cell. The horizontal arrows indicate the four-membered rings. A, B, and C indicate the three atomic chains along the ⟨211⟩ direction in the CSL unit cell.

$abcc'b'$ and seven-membered rings such as $abcc'f'fe$. Between chains A and C, there exist only six-membered rings.

This configuration contains two kinds of twofold symmetry. Thus there exist four atoms that are symmetrically equivalent to each other, respectively, in the CSL unit cell, and the interface atoms can be classified into six atomic groups. Atoms of one four-membered ring and neighboring atoms are labeled $a-f$ in Fig. 7, and symmetrically equivalent atoms are indicated as a and a', for example. The respective two atoms in the four-membered ring are equivalent to each other. Chain C is equivalent to chain A by the symmetry, and thus the two four-membered rings in chains A and C are equivalent to each other.

The bond-length and bond-angle distortions in this configuration range from -2.4 to $+2.0\%$ and from $-35.5°$ to $+28.5°$, respectively. Relatively large bond distortions, especially large bond-angle distortions, are associated with the four-membered rings. The bond-angle distortions of the four-membered ring at atoms a and a' are $-35.5°$, and those at atoms b and b' are $-15.2°$. The bond-angle distortions at angles $\angle bae$ and $\angle b'a'e'$ are $+28.5°$. Bonds ab and $a'b'$ at the four-membered ring are stretched by $+2.0\%$, and bonds ab' and $a'b$ are stretched by $+1.9\%$. The back bonds of the four-membered ring, bd and $b'd'$, are contracted by -2.4%, and the back bonds ae and $a'e'$ are stretched by $+1.7\%$.

Figure 8 shows the band structure and boundary-localized states of this configuration. The boundary-localized states exist at the lower edge of the valence band, at the upper edge of the valence band, and at the lower edge of the conduction band. It is clear that the boundary-localized states exist inside the minimum band gap because of the great degree of structural disorder of the present configuration. The uppermost states at the valence-band edge exist above the valence-band maximum by about 0.17 eV, and the lowest states at the conduction-band edge exist below the conduction-band minimum by about 0.01 eV.

Figure 9 shows LDOS's of the interface atoms. In the LDOS's of atoms a and b of the four-membered rings, similar remarkable changes exist. In both the LDOS's, a sharp s-like peak is generated at the bottom of the valence band instead of the ordinary s-like peak, and a sharp p-like peak is shifted toward the band gap. Between these two peaks, the shape of the valence-band DOS is rather smooth due to increases at the two valleys and a decrease of the s-p mixing peak. The DOS's are also increased at the top of the valence band and the bottom of the conduction band.

The increases at the top of the valence band and the bottom of the conduction band are also observed in the LDOS's of the neighboring atoms of the four-membered
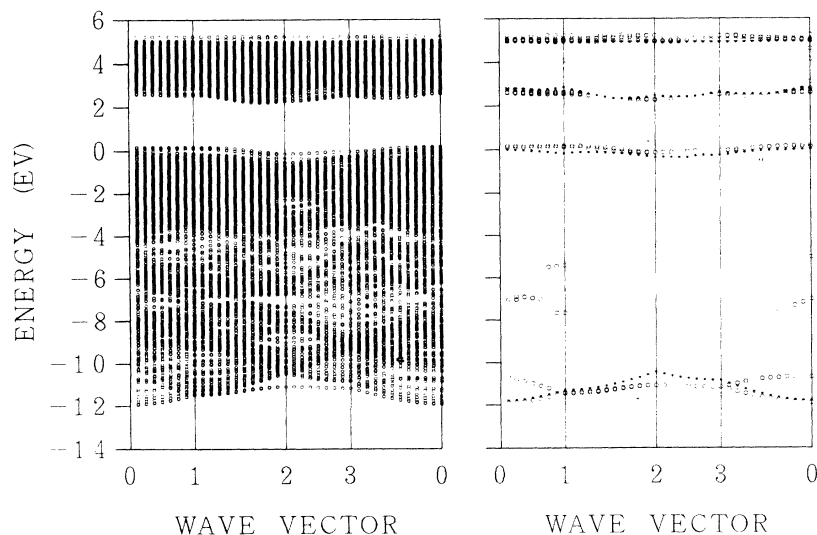
FIG. 8. Band structure and boundary-localized states of the ⟨011⟩ Σ=3 twist boundary in Si shown in Fig. 7. In the left panel, all the eigenstates of the supercell are plotted along the lines in the two-dimensional Brillouin zone. In the right panel, the states for which the probability that an electron is located on the atoms of the four (011) atomic layers at the interface exceeds 75% are plotted. The dotted curves indicate the projected band edges of the perfect crystal. Points 0, 1, 2, and 3 correspond to $(0, 0, 0)$, $(\pi/|\mathbf{R}_1|,0,0)$, $(\pi/|\mathbf{R}_1|,\pi/|\mathbf{R}_2|,0)$, and $(0,\pi/|\mathbf{R}_2|,0)$ in the Brillouin zone of the supercell, where $|\mathbf{R}_1|=\sqrt{3}a_0$ and $|\mathbf{R}_2|=\sqrt{6}a_0/2$.

rings, c, d, and e, as shown in Fig. 9, although the total changes of the LDOS's are not so large compared with the atoms in the four-membered rings. In the LDOS's of atoms c and d, there exists a distinct small s-like peak or a slight increase at the bottom of the valence band similar to the LDOS's of four-membered rings.

The additional peaks or increases at the band edges in the LDOS's observed at the four-membered rings and neighboring atoms should correspond to the generation of the boundary-localized states, as shown in Fig. 8. We have analyzed the distributions of such boundary-localized states, as shown in Table I. Large portions of the boundary-localized states at the bottom of the valence band exist among atoms b, a, c, and d, and symmetrically equivalent atoms. This is in good agreement with the distinct peaks or increases at the bottom of the valence band in the LDOS's of these atoms in Fig. 9. Large portions of the boundary-localized states at the top of the valence band exist among atoms a, b, d, and e, and equivalent atoms. Large portions of the boundary-localized state at the bottom of the conduction band exist among atoms a, b, c, and e, and equivalent atoms. These results are also in good agreement with increases at the top of the valence band in the LDOS's of atoms a, b, d, and e, and at the bottom of the conduction band in the LDOS's of atoms a, b, c, and e in Fig. 9, respectively.

It is clear that large portions of the respective boundary-localized states exist among the four-membered rings and neighboring atoms. It seems that the genera-

tion of these boundary-localized states is caused mainly by four-membered rings. However, four-membered rings inevitably contain large bond-angle distortions. Thus it is probable that the boundary-localized states at the top of the valence band and the bottom of the conduction band are essentially caused by such large bond-angle distortions, as well as the band-edge states of the $\langle 111 \rangle$ $\Sigma = 7$ boundary shown in Sec. III B, rather than the pure topological effects of four-membered rings.

However, the unique combination of both sharp peaks at the bottom and top of the valence band coupled with the rather smooth shape between these two peaks in the LDOS's seems to be characteristic of four-membered rings. This is because similar features of the LDOS's are observed at atoms of four-membered rings also in other interfaces, as will be shown in Sec. III D and in paper III. Of course, the dehybridization caused by large bond-angle distortions at four-membered rings might be concerned with these features, and associated odd-membered rings might be concerned with the rather smooth shape between the two peaks.

In any case, it is clear that four-membered rings or associated large bond-angle distortions generate electronic states at the bottom and top of the valence band and at the bottom of the conduction band, which become boundary-localized states when they exist in the forbidden energy regions of the bulk crystal.

Again, boundary-localized states are not sharply localized to specific atoms, but are distributed rather widely in
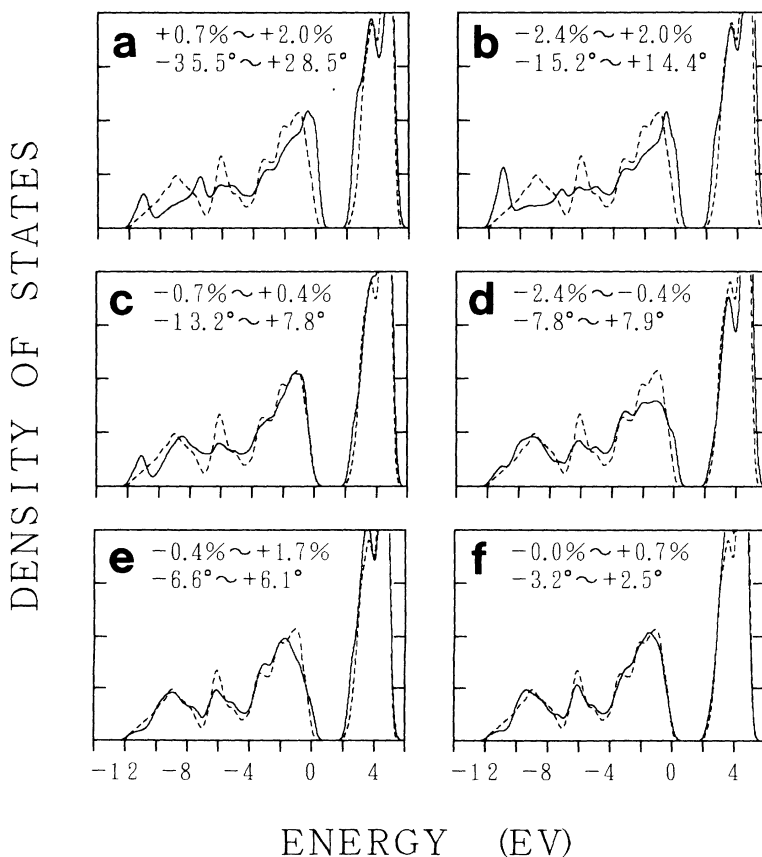
FIG. 9. LDOS's of the interface atoms in the $\langle 011 \rangle$ $\Sigma = 3$ twist boundary in Si in Fig. 7. LDOS's of the atoms labeled in Fig. 7 are shown. The dashed lines indicate the bulk density of states, which is obtained by the LDOS of the central atom in the supercell. The ranges of the bond-length and bond-angle distortions associated with the respective atoms are also shown.

directions parallel to the interface, as found in the analysis of the distributions. Thus the present boundary-localized states are localized only in the direction normal to the interface, similarly to those of the $\langle 111 \rangle$ $\Sigma = 7$ boundary. As will be discussed in Sec. IV C, the reason for the small degree of localization in directions parallel to the interface seems to be, as in the case of the $\langle 111 \rangle$ $\Sigma = 7$ boundary, that similar bond distortions or four-membered rings are arranged with a high density or with short periods in the interface, as well as the effects of the symmetric property of the present configuration.

Finally, regarding the effects of odd-membered rings, it should be noted that atoms a, b, and c belong to both the five- and seven-membered rings. In LDOS's of these atoms, it seems that shapes at the s-p mixing peak and at the two valleys of the valence-band DOS can be explained by the effects of odd-membered rings, as discussed in Sec. III A, although there exists the complexity that atoms a and b are also members of four-membered rings. We have analyzed the boundary-localized states at about -5 and -7 eV within the valence band in Fig. 8, and found

that large portions of these states indeed exist among atoms a, b, and c, and equivalent atoms.

D. The $\langle 011 \rangle$ $\Sigma = 3$ twist boundary: weak bond

Figure 10 shows the relaxed configuration of the $\langle 011 \rangle$ $\Sigma = 3$ twist boundary with the other translation. The translation parallel to the interface is $R_2/12$ (Trans. 4 in paper I) and the optimized translation normal to the interface is $+0.1$ Å. E_{gb} is 1.21 J/m^2. The bond-length and bond-angle distortions range from -1.7 to $+8.1\%$, and from $-28.9°$ to $+24.2°$, respectively.

The present configuration contains only one kind of twofold symmetry, and the equivalent atoms are indicated as a and a', for example, in Fig. 10. In the CSL unit cell, there exist three atomic chains along the $\langle 211 \rangle$ direction denoted by A, B, and C in Fig. 10. Chains A and B contain only six-membered rings. Chain C contains four-membered rings such as $de'd'e$ and eight-membered rings. Between chains A and B, four-

TABLE I. Examples of the distributions of wave functions of the boundary-localized states of the $\langle 011 \rangle$ $\Sigma = 3$ twist boundary in Si in Fig. 7. Typical boundary-localized states at points 1 and 0 in Fig. 8 are analyzed. Distributions to respective atoms in the CSL unit cell larger than 3% are listed. Atoms are labeled similarly to Fig. 7. Note that distributions to symmetrically equivalent atoms (total four atoms in the CSL unit cell) are all the same due to the symmetric property of the wave functions. Thus the listed values of probabilities are common for each symmetric atom.

k vector	Energy	Distributions
Bottom of the valence band		
1	-11.47 eV	b and symmetric atoms:7.2%; a and symmetric atoms:5.7%; d and symmetric atoms:4.0%
1	-11.42 eV	c and symmetric atoms:7.0%; b and symmetric atoms:5.9%
0	-11.91 eV	b and symmetric atoms:5.4%; c and symmetric atoms:3.7%; a and symmetric atoms:3.7%
0	-10.69 eV	b and symmetric atoms:12.0%; a and symmetric atoms:6.0%; c and symmetric atoms:3.3%
Shallow band-edge states		
Top of the valence band		
1	0.11 eV	b and symmetric atoms:6.7%; a and symmetric atoms:6.6%; d and symmetric atoms:4.9%
1	0.16 eV	a and symmetric atoms:6.5%; b and symmetric atoms:6.0%; d and symmetric atoms:4.4%
0	0.10 eV	b and symmetric atoms:6.6%; a and symmetric atoms:6.5%; d and symmetric atoms:5.2%
0	0.17 eV	a and symmetric atoms:6.6%; b and symmetric atoms:6.3%; d and symmetric atoms:3.8%; e and symmetric atoms:3.1%
Bottom of the conduction band		
1	2.56 eV	a and symmetric atoms:7.3%, b and symmetric atoms:7.1%
1	2.64 eV	e and symmetric atoms:7.2%, a and symmetric atoms:6.8%; b and symmetric atoms:4.1%
0	2.63 eV	e and symmetric atoms:7.3%, a and symmetric atoms:6.0%, b and symmetric atoms:4.1%
0	2.64 eV	a and symmetric atoms:7.4%, b and symmetric atoms:6.7%, c and symmetric atoms:4.1%

⟶ [1̄1̄1]
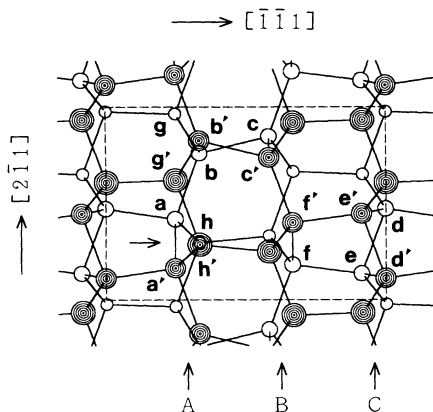
FIG. 10. Relaxed atomic configuration of the ⟨011⟩ Σ=3 twist boundary in Si with the rotation angle 109.5° and Trans. 4. Atomic positions of the four (011) atomic layers are projected along the ⟨011⟩ axis, and open and closed circles indicate the atoms of the lower and upper crystals, respectively. The dashed lines indicate the CSL unit cell. The horizontal arrow indicates the greatly stretched bond by 8.1%. *A*, *B*, and *C* indicate the three atomic chains along the ⟨211⟩ direction in the CSL unit cell.

membered rings such as *bb'c'c* and eight-membered rings are contained. Between chains *A* and *C*, and *B* and *C*, five-membered rings such as *aa'd'ed* or *ff'e'd'e* and seven-membered rings are contained. There exist two four-membered rings in the CSL unit cell.

Bond *aa'*, indicated by an arrow in Fig. 10, is greatly stretched by +8.1%. Also, large bond-angle distortions ranging from −12.0° to +24.2° are associated with these atoms. Bond *ff'* is also stretched by +3.8%. Relatively large bond distortions are associated with four-membered rings. At the four-membered ring *bb'c'c*, bonds *bc* and *b'c'* are stretched by +2.6%. Back bonds *ba* and *b'a'* are stretched by +2.7%, back bonds *bg* and *b'g'* are stretched by +1.4%, and back bonds *cf* and

c'f' are stretched by +1.0%. Bond-angle distortions of the four-membered ring *bb'c'c* are −23.1° and −22.7° at corners *b* and *b'* and *c* and *c'*, respectively. Bond-angle distortions as large as +19.7° and +16.1° are associated with the back bonds. The four-membered ring *de'd'e* does not contain large bond-length distortions, but contains bond-angle distortions as large as −28.9° at corners *d* and *d'* and −23.5° at corners *e* and *e'*, respectively, with bond-angle distortions as large as +22.4° and +17.8° associated with the back bonds.

Figure 11 shows the band structure and boundary-localized states of the present configuration. The boundary-localized states are generated at the bottom of the valence band, at the top of the valence band, and at the bottom of the conduction band. It is remarkable that two bands are generated inside the band gap above the valence-band maximum and below the conduction-band minimum. The lower band is occupied, and the upper band is empty. Both bands have small dispersion; the lower band ranges from 0.06 to 0.38 eV, and the upper band ranges from 1.85 to 2.37 eV. As shown in the right panel of Fig. 11, there also exist shallower states associated with the band edges, similar to band-edge states of the other interfaces described above. It is clear that the two bands inside the band gap and the shallow band-edge states can be distinguished, although the tendency of hybridization between these two kinds of states can be seen near point 2 and point 0 in Fig. 11.

Figure 12 shows LDOS's of the interface atoms. Symmetrically equivalent atoms have the same LDOS's. Table II shows examples of the distributions of the boundary-localized states shown in Fig. 11. Analyses of the LDOS's and the distributions of the boundary-localized states indicate that the two bands inside the band gap are caused mainly by the greatly stretched *aa'* bond, and that these states can be regarded as so-called weak-bond states. It has also been found that shallow band-edge states and the other changes in the LDOS's are mainly caused by the remaining structural disorder in a fashion similar to that described in preceding subsections.
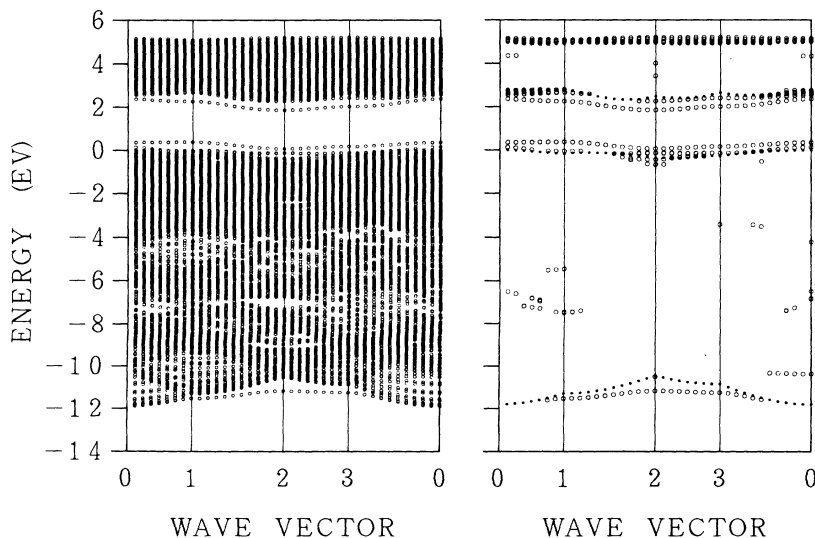
FIG. 11. Band structure and boundary-localized states of the ⟨011⟩ Σ=3 twist boundary in Si shown in Fig. 10. In the left panel, all the eigenstates of the supercell are plotted along the lines in the two-dimensional Brillouin zone. In the right panel, the states for which the probability that an electron is located on the atoms of the four (011) atomic layers at the interface exceeds 75% are plotted. The dotted curves indicate the projected band edges of the perfect crystal. Points 0, 1, 2, and 3 correspond to (0, 0, 0), $(\pi/|\mathbf{R}_1|, 0, 0)$, $(\pi/|\mathbf{R}_1|, \pi/|\mathbf{R}_2|, 0)$, and $(0, \pi/|\mathbf{R}_2|, 0)$ in the Brillouin zone of the supercell, where $|\mathbf{R}_1| = \sqrt{3}a_0$ and $|\mathbf{R}_2| = \sqrt{6}a_0/2$.

The electronic states of the two bands inside the band gap are much more localized at specific atomic sites (a, a', b, and b') than other electronic states. As shown in Fig. 12, the LDOS's of atoms a and b contain peaks corresponding to these two bands, although the large portion of the peak at the bottom of the conduction band in the LDOS of atom b is also concerned with the shallow band-edge states. The LDOS's of the other atoms do not reveal marked peaks corresponding to these two bands, although small increases at the position of the lower band are observed in LDOS's of the neighboring atoms h, h', g, and g' in chain A. The peak at the top of the valence band in the LDOS of atom c in Fig. 12 is concerned mainly with the shallow band-edge states as mentioned below, although it contains small portions of the states of the lower band.

The distributions of the states of the two bands shown in Table II indicate clearly that large portions of the respective states of the lower band exist at atoms b, b', a, and a' as well as small portions at atoms h and h', and

that large portions of the respective states of the upper band exist at atoms a and a' as well as small portions at atoms b and b'.

The degree of localization of these states in directions parallel to the interface is most marked among all the boundary-localized states in the present paper. As shown in Table II, the probabilities over 50% of these respective states exist among atoms a and a' or among atoms a, a', b, and b', although the degree of localization of the states of the lower band seems to be a little less than that of the upper band. Of course, atoms a, a', b, and b' constitute a zigzag chain along the $\langle 211 \rangle$ direction, and are repeated with a short period. Thus the states of these two bands cannot be regarded as strictly localized along this chain. This is consistent with the substantial dispersion of these two bands along the $\langle 211 \rangle$ direction, namely the dispersion between points 1 and 2, and between points 3 and 0 in Fig. 11. However, these states can be regarded as substantially localized along the $\langle 111 \rangle$ direction as well as in the direction normal to the interface, because the distri-
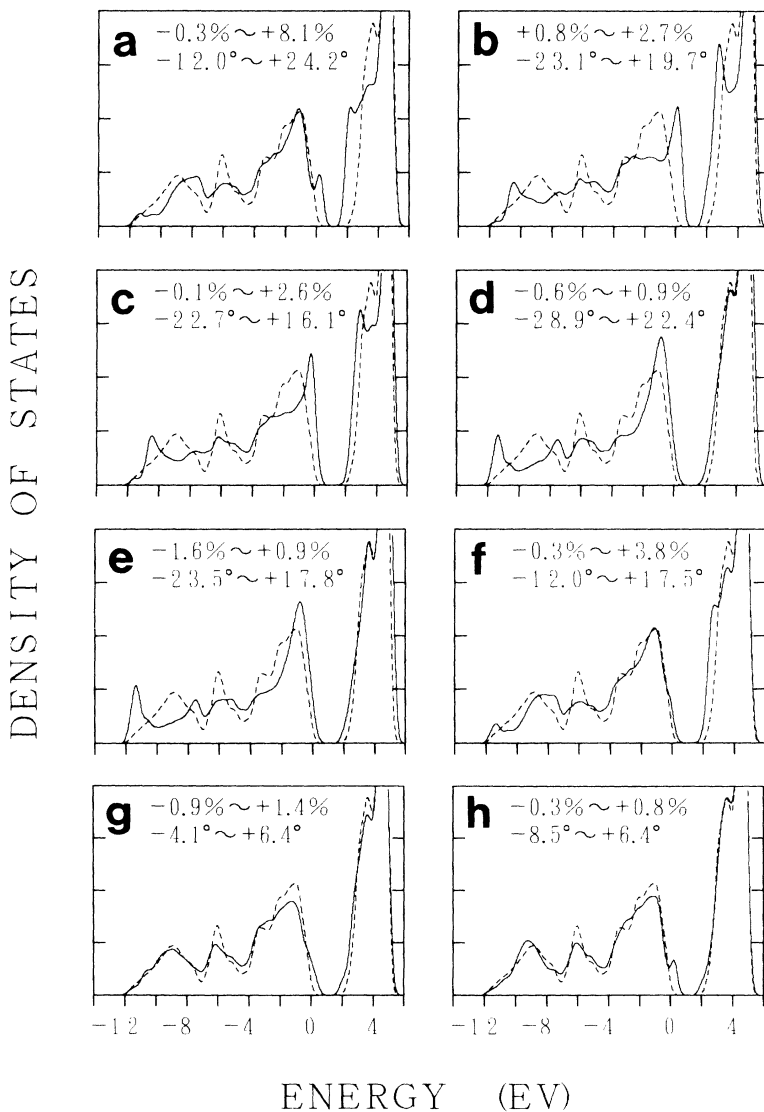
FIG. 12. LDOS's of the interface atoms in the $\langle 011 \rangle$ $\Sigma = 3$ twist boundary in Si in Fig. 10. LDOS's of the atoms labeled in Fig. 10 are shown. The dashed lines indicate the bulk density of states, which is obtained by the LDOS of the central atom in the supercell. The ranges of the bond-length and bond-angle distortions associated with the respective atoms are also shown.

TABLE II. Examples of the distributions of wave functions of the boundary-localized states of the ⟨011⟩ Σ=3 twist boundary in Si in Fig. 10. Typical boundary-localized states at points 1, 2, and 0 in Fig. 11 are analyzed. Distributions to respective atoms in the CSL unit cell larger than 3% are listed. Atoms are labeled similarly to Fig. 10. Atoms *i*-1 and symmetric atoms not indicated in Fig. 10 are the neighbors of the atoms *c*-*f* in Fig. 10, respectively. Note that distributions to symmetrically equivalent atoms (total two atoms in the CSL unit cell) are all the same due to the symmetric property of the wave functions. Thus the listed values of probabilities are common for each symmetric atom.

k vector	Energy	Distributions
Weak-bond states		
Lower band		
1	0.37 eV	*b* and *b'*:18.5%; *a* and *a'*:9.7%; *h* and *h'*:8.2%; *g* and *g'*:3.9%
2	0.06 eV	*b* and *b'*:19.5%; *a* and *a'*:9.7%; *c* and *c'*:4.3%; *h* and *h'*:3.7%
0	0.35 eV	*b* and *b'*:17.4%; *a* and *a'*:9.8%; *h* and *h'*:7.7%; *g* and *g'*:4.0%
Upper band		
1	2.27 eV	*a* and *a'*:21.3%; *b* and *b'*:6.1%; *e* and *e'*:4.5%; *f* and *f'*:3.9%; *d* and *d'*:3.8%
2	1.85 eV	*a* and *a'*:21.2%; *b* and *b'*:7.9%; *g* and *g'*:3.4%
0	2.37 eV	*a* and *a'*:28.8%; *b* and *b'*:7.5%; *e* and *e'*:3.4%
Shallow band-edge states		
Top of the valence band		
1	−0.05 eV	*c* and *c'*:15.2%; *f* and *f'*:7.6%; 1 and 1':6.9%; *i* and *i'*:4.3%
2	−0.43 eV	*d* and *d'*:12.9%; *e* and *e'*:12.8%; *b* and *b'*:7.0%; *c* and *c'*:4.5%; *k* and *k'*:4.0%
	−0.15 eV	*c* and *c'*:11.2%; *b* and *b'*:11.2%; *g* and *g'*:3.9%; *d* and *d'*:3.6%; *e* and *e'*:3.6%; *i* and *i'*:3.4%; *a* and *a'*:3.3%
0	0.14 eV	*d* and *d'*:7.3%; *e* and *e'*:7.3%; *b* and *b'*:6.3%; *c* and *c'*:5.9%; *k* and *k'*:4.6%; *j* and *j'*:4.0%
Bottom of the conduction band		
1	2.68 eV	*f* and *f'*:10.5%; *b* and *b'*:7.6%; *c* and *c'*:5.1%; *a* and *a'*:5.1%; *d* and *d'*:4.3%
1	2.81 eV	*b* and *b'*:13.3%; *g* and *g'*:8.1%; *a* and *a'*:5.7%; *f* and *f'*:4.7%
2	2.28 eV	*f* and *f'*:12.5%; *c* and *c'*:8.1%; *b* and *b'*:4.4%; *a* and *a'*:4.2%; *d* and *d'*:3.1%
0	2.56 eV	*b* and *b'*:12.5%; *a* and *a'*:10.5%; *c* and *c'*:4.8%; *g* and *g'*:4.2%; *e* and *e'*;4.0%; *j* and *j'*:3.5%; *d* and *d'*:3.1%
0	2.64 eV	*f* and *f'*:15.3%; *b* and *b'*:5.7%; *d* and *d'*:4.7%; *c* and *c'*:4.3%; *g* and *g'*:3.2%
0	2.77 eV	*c* and *c'*:10.4%; *f* and *f'*:7.8%; *d* and *d'*:5.2%; *b* and *b'*:5.0%; *e* and *e'*:3.7%; *k* and *k'*:3.7%
Bottom of the valence band		
1	−11.53 eV	*e* and *e'*:12.7%; *d* and *d'*:11.0%; *k* and *k'*:4.0%; *f* and *f'*:3.9%; *j* and *j'*:3.8%
2	−11.18 eV	*e* and *e'*:19.2%; *d* and *d'*:16.4%; *f* and *f'*:5.3%; *a* and *a'*:3.3%
	−10.51 eV	*c* and *c'*:14.1%; *b* and *b'*:12.2%; *i* and *i'*:4.9%
0	−10.38 eV	*c* and *c'*:10.2%; *b* and *b'*:8.8%; *e* and *e'*:4.5%; *d* and *d'*:4.1%

butions to chains B and C are small, and the dispersion of these two bands along the $\langle 111 \rangle$ direction, namely between points 0 and 1 and between points 2 and 3 in Fig. 11, is small.

It is clear that the states of these two bands are mainly localized at the greatly stretched bond aa' and the neighboring atoms b and b', and it can be said that the generation of these two bands is caused mainly by the greatly stretched bond. Here it can be considered that the present two bands should become truly localized states without any dispersion inside the band gap, if the size of the CSL unit cell becomes infinitely large along the $\langle 211 \rangle$ and $\langle 111 \rangle$ directions with only one such greatly stretched bond in the unit cell. Thus these two bands can be regarded as so-called weak-bond states, in marked contrast to the shallow band-edge states of the present interface and those of the other interfaces described above. The lower and upper bands correspond to the bonding and antibonding states of the weak bond, respectively.

Ideally, it can be considered that weak-bond states have features intermediate between deep dangling-bond states and shallow band-edge states. Weak-bond states are deeper inside the band gap and more localized to specific atoms than shallow band-edge states. However, in contrast to dangling-bond states analyzed in paper III, weak-bond states consist of an occupied bonding and an unoccupied anti-bonding state and are not so deep in the band gap. Naturally, the energy levels of weak-bond states should depend on the degree of bond distortions. During lattice relaxation, we have found that the position of the lower band becomes gradually shallower in accordance with the relaxation of the bond distortions at and around the weak bond.

As will be discussed in Sec. IV C, we think the following two points are necessary conditions for the ideal weak-bond states localized well in directions parallel to the interface, as well as in the direction normal to the interface. First, the degree of bond distortions must be sufficient to drive the states deeper inside the band gap. Second, such a greatly distorted bond must be isolated or sparsely distributed in the interface without similar neighboring distortions. This isolation should cause a great degree of localization. In the present case, the second condition is not completely satisfied because of the repetition of the cells, especially along the $\langle 211 \rangle$ direction.

On the other hand, all LDOS's at four-membered rings in the present configuration have characteristics similar to those observed in Sec. III C. As shown in the LDOS's of atoms $b-e$ in Fig. 12, sharp s- and p-like peaks are generated at the bottom and top of the valence band, and the shape of the valence band between these two peaks is rather smooth. It seems that these particular changes in the LDOS's are the general effects of four-membered rings, although the associated large bond-angle distortions may be the essential cause of such changes rather than pure topological effects as discussed in Sec. III C.

The shallow band-edge states distinguished from the weak-bond states in the right panel of Fig. 11 are caused mainly by large bond-angle distortions of the four-membered rings, as well as the similar band-edge states

analyzed in Sec. III C. As shown in Table II, large portions of the respective shallow band-edge states are indeed distributed on the four-membered rings and neighboring atoms. Distributions of the states at the top of the valence band are consistent with increases in the LDOS's of atoms b, c, d, e, and f in Fig. 12, although the increases at atoms b, and c in Fig. 12 are partially concerned with the lower weak-bond states, as mentioned above. Distributions of the states at the bottom of the conduction band are also consistent with increases in the LDOS's of atoms b, c, d, f, and g in Fig. 12. There exist relatively large distributions of the shallow band-edge states to atoms f and f' as compared with other neighboring atoms of the four-membered rings. This seems to be concerned with the relatively large stretching of $+3.8\%$ at bond ff'.

The tendency of localization of these shallow band-edge states to specific atoms is not very large compared with weak-bond states. For example, for weak-bond states, probabilities over 50% exist among atoms a and a' or among atoms a, a', b, and b' in the CSL unit cell. For shallow band-edge states, probabilities over 50% are distributed over six or eight atoms in the CSL unit cell. Further, the maximum distributions for respective atoms are not so large as compared with the weak-bond states. Thus the degree of localization in directions parallel to the interface of the shallow band-edge states is small, and these states are localized only in the direction normal to the interface, as for similar band-edge states described in Secs. III B and III C. This feature, discriminating shallow band-edge states from weak-bond states, can be understood by the two conditions mentioned above.

The tendency of hybridization between shallow band-edge states and weak-bond states is observed at the valence-band edge at point 2, and at the conduction-band edge at point 0 in Fig. 11, where the energy levels of the two kinds of states are near each other. For example, as shown in Table II, large portions of one of the shallow band-edge states of 2.56 eV at point 0 also exist at the weak bond aa' as well as among the four-membered rings and neighboring atoms.

On the other hand, about the boundary-localized states at the bottom of the valence band in Fig. 11, large portions of the respective states exist mainly among the atoms of the four-membered rings, as in the case of similar states in Sec. III C. As shown in Table II, a series of boundary-localized stats ranging from -11.5 to -11.2 eV in Fig. 11 are mainly localized at the four-membered ring $ed'e'd$. There also exist states localized mainly at the four-membered ring $bb'c'c$ at about -10.4 eV, as shown in Table II. These results are consistent with sharp s-like peaks at about -11.5 eV in the LDOS's of atoms d and e in Fig. 12, and those at about -10.4 eV in the LDOS's of atoms b and c in Fig. 12.

Finally, regarding the effects of odd-membered rings, a tendency similar to that found in the $\Sigma = 9$ boundary seems to exist in LDOS's of members of both the five- and seven-membered rings, although the effects cannot be examined clearly due to the complexity of the configuration. For example, we have found that relatively large portions of the boundary-localized states of about

−7.5 eV at point 1 in Fig. 11 exist among atoms f, f', e, e', a, a', d, and d', which are members of both the five- and seven-membered rings. This is consistent with the distinct increases at the valleys in the LDOS's of these atoms in Fig. 12.

IV. DISCUSSION

A. Effects of structural disorder on the local electronic structure of Si

The present calculations of tilt and twist boundaries have shown the effects of various kinds of structural disorder, with the exception of coordination defects, on the local electronic structure of Si. Odd-membered rings induce the changes in the LDOS's of associated atoms, particularly atoms belonging to both five- and seven-membered rings. The LDOS's are increased at the two valleys among the three peaks of the valence-band DOS, and are decreased at the s-p mixing peak. There is also a slight shift of the p-like peak toward the band edge, which may be more related to the associated bond distortions than to topological effects. Bond stretchings and bond-angle distortions generate electronic states at the top of the valence band and the bottom of the conduction band, thus inducing peaks at the band edges in the LDOS's of the distorted atoms. These states become boundary-localized states, especially as they are pushed into the gap. Four-membered rings induce a peculiar shape in the LDOS's where sharp s- and p-like peaks are generated at the bottom and top of the valence band, respectively, and the density between these two peaks is rather smooth. It also seems that large bond-angle distortions associated with four-membered rings generate shallow band-edge states at the top of the valence band and the bottom of the conduction band. Greatly stretched bonds generate so-called weak-bond states, of which bonding and antibonding states exist inside the minimum band gap. The weak-bond states are deeper in the band gap and more spatially localized than the shallow band-edge states caused by smaller bond distortions. The effects of dihedral-angle distortion do not seem to be so pronounced, although this distortion seems to be associated with a slight shift of the p-like peak toward lower energy in the LDOS.

It can be said that the depth in the band gap of the band-edge states caused by bond distortions depends on the degree of bond distortions. This point has been clarified in the comparison between shallow band-edge states and weak-bond states, and in our observations of the electronic states during the procedure of lattice relaxation. This may explain why band-edge states in the CSL tilt boundaries do not penetrate into the minimum band gap,[10−18] in contrast to those of the present twist boundaries. From present calculations of the CSL tilt and twist boundaries, and previous calculations of the CSL tilt boundaries in Si,[10,11,13−17] a critical value of bond stretchings for the generation of states inside the minimum band gap in Si seems to be about several percent. Such a critical absolute value of bond-angle distortions seems to be in the range from 25° to 30°. In the present ⟨111⟩ $\Sigma=7$ boundary, bond stretchings as large

as +4.6% associated with bond-angle distortions as large as −23.5° generate states inside the minimum band gap, in particular at the conduction-band edge. In the ⟨011⟩ $\Sigma=3$ boundary in Sec. III C, bond-angle distortions as large as −35.5° associated with four-membered rings generate states inside the minimum band gap, in particular at the valence-band edge. Of course, it is probable that the generation of such states is dominated not only by such critical values but also by the density of such distortions or the combination of bond-length and bond-angle distortions. For example, in the calculation of the facet junction between {211} $\Sigma=3$ and {111} $\Sigma=3$ boundaries in Si,[24] large bond-angle distortions over 30° arranged linearly along the ⟨011⟩ axis do not generate electronic states penetrating into the minimum band gap, while states associated with the conduction-band edge are generated.

Comparing band-edge states at the top of the valence band with those at the bottom of the conduction band caused by bond distortions, we find the tendency for boundary-localized states to be generated frequently at the conduction-band edge rather than at the valence-band edge, as in the cases of the present $\Sigma=7$ and $\Sigma=9$ boundaries and previously calculated CSL tilt boundaries in Si,[11,15] although there exist examples containing both kinds of band-edge states. The same tendency has been observed recently in *ab initio* calculation of the {310} $\Sigma=5$ tilt boundary in Ge.[18] As pointed out in Ref. 18, this seems to be consistent with experiments indicating that traps for electrons, not holes, frequently exist in grain boundaries in Ge,[47] although such states do not seem to be intrinsic states of CSL boundaries.

We believe that this tendency is caused by the fact that the reconstruction or relaxation of interface configurations is performed so as to decrease the total energy associated with the occupied electronic states. In the relaxation, the bond distortions should be relaxed so as to decrease the occupied gap states or occupied band-edge states. Thus the valence-band-edge states should be decreased directly, although the decrease of the unoccupied conduction-band-edge states should only be indirect, and the latter may frequently remain. We think that this is the reason for the aforementioned trend in the calculated results, and that this may also be the reason behind the experimental results for Ge.

B. Comparison with theoretical results of amorphous Si

We think the present results can be regarded as general effects of structural disorder on the local electronic structure of Si, and applied to general disordered systems such as amorphous Si. Various theoretical studies have been performed[32−43] in order to clarify the effects of structural disorder in amorphous Si. It should be noted that the configurations of grain boundaries in this paper are very effective in clarifying the effects of respective kinds of structural disorder on the bulk electronic structure of Si, because the respective kinds of disorder can be arranged and buried properly between the bulk crystals in the configurations of grain boundaries.

Changes in DOS's similar to those found in the present

{122} $\Sigma=9$ boundary have also been attributed to the effects of odd-membered rings in electronic structure calculations of hypothetical crystalline polymorphs of Si such as ST-12.[32,33] However, these effects are demonstrated much more clearly in the present grain boundary calculations, because only the odd-membered rings are properly buried and arranged between the perfect crystals without large bond distortions in the present configuration of the {122} $\Sigma=9$ boundary. We have also provided an example without any odd-membered rings (the $\langle 111 \rangle$ $\Sigma=7$ boundary) in which we find no such changes in the LDOS's.

The present results about the effects of bond stretchings and bond-angle distortions found in the $\langle 111 \rangle$ $\Sigma=7$ boundary, and the effects of bond-angle distortions at four-membered rings found in the $\langle 011 \rangle$ $\Sigma=3$ boundary, are consistent with previous theoretical results of amorphous Si. In studies using the Bethe lattice method with the tight-binding Hamiltonian,[34,35] bond stretchings generate states at the top of the valence band and the bottom of the conduction band, and bond-angle distortions generate states at the top of the valence band and the bottom of the conduction band as well. The present calculations of twist boundaries have shown the effects of bond distortions in Si clearly by using realistic atomic configurations and Hamiltonian.

The x-ray photoemission spectroscopy (XPS) observation[48] of the valence-band DOS of amorphous Si can be explained by the present theoretical results. In the observed DOS, the two lower peaks of the valence band merge into a single featureless hump. The p-like peak is shifted toward the band edge, steepening the shape of the DOS at the band edge. The former effect can be understood now as an effect coming from odd-membered rings, and the latter effect can be understood now as an effect of bond distortions. Of course, the latter may also be attributed to bond distortions associated with odd-membered rings in a way similar to the slight shift observed in the {122} $\Sigma=9$ boundary.

Regarding dihedral-angle disorder and odd-membered rings, Cohen et al.[36] and Singh[37] have emphasized the effects of such kinds of disorder on the valence-band edge and on the conduction-band edge in amorphous Si. By analysis of eigenstates at the band edges using the tight-binding Hamiltonian, they pointed out that states at the top of the valence band of the bulk crystal are suppressed by dihedral-angle disorder, and states at the bottom of the conduction band of the bulk crystal are also suppressed by odd-membered rings. Thus the states localized to bulklike regions are generated at the band edges in amorphous Si.

It should be noted that their argument is intended to clarify the origins of states localized not to distorted regions but to bulklike regions surrounded by distorted regions in amorphous Si, of which energy levels should exist inside the bands between the bulk band edge and mobility edge. Thus their argument cannot be applied straightforwardly to the present case of grain boundaries with bulk crystals on both sides. Localization to bulklike regions does not seem to occur in the case of grain boundaries with widths that are not so large.

However, in the present LDOS of the atom with only dihedral-angle disorder in the $\langle 111 \rangle$ $\Sigma=7$ boundary shown in Fig. 6, there exists a slight shift of the p-like peak toward lower energy. This change seems to be consistent with the above argument that bulklike states at the top of the valence band are suppressed by dihedral-angle disorder. About the effects of odd-membered rings in the above argument, there exist indeed some decreases at the lower peak of the conduction band in the LDOS's of the interface atoms of the {122} $\Sigma=9$ boundary shown in Fig. 3. These changes may be concerned with the suppression of the bulklike states at the bottom of the conduction band by odd-membered rings.

About weak bonds and four-membered rings in amorphous Si, an electronic structure calculation[38] has been performed using the SETB method[44] with a supercell configuration, and such kinds of disorder have also been analyzed as coordination defects. Weak bonds, four-membered rings with large bond-angle distortions, and individual atoms with large bond-length or bond-angle distortions, have been found to generate shallow states at the band edges, although detailed analyses have not been given. These results are consistent with the present results.

Recently, more quantitative calculations have been performed about the atomic and electronic structures of amorphous Si by using first-principles band-structure calculations coupled with supercell configurations.[39-41] However, in such calculations, various kinds of structural disorder are contained complicatedly with very high densities or with very short periods because of the small cells. Thus, as shown in Refs. 39 and 41, it is not easy to analyze the effects of respective kinds of structural disorder. As mentioned above, one of the advantages of the present calculations exists in this point.

C. Nature of boundary-localized states

As shown in Sec. III, the present tilt and twist boundaries contain various boundary-localized states. These boundary-localized states can be classified into two groups. The first group is the states that are localized in interface layers only in the sense that the wave functions do not propagate into the bulk regions. These states are not localized in directions parallel to the interface. The second group is states that have a great degree of localization in directions parallel to the interface as well as normal to the interface. The boundary-localized states in the {122} $\Sigma=9$ boundary and the shallow band-edge states in the $\langle 111 \rangle$ $\Sigma=7$ and $\langle 011 \rangle$ $\Sigma=3$ boundaries fall in the first group. The weak-bond states in the $\langle 011 \rangle$ $\Sigma=3$ boundary can be classified into the second group. Of course, no states are strictly localized in directions parallel to the interface in CSL boundaries with two-dimensional periodicity, and there exists no sharp separation between these two groups in calculations of CSL boundaries.

As discussed in Sec. III D, we believe that the two conditions necessary for generating well-localized states of the second group are, first, that the degree of bond distortions be sufficient to cause electronic states inside the

minimum band gap and, second, that such bond distortions be isolated or distributed sparsely without neighboring similar bond distortions in the interface. These two conditions should be correlated with each other. It seems that greater bond distortions induce a greater tendency for localization of the generated states, as well as deeper levels of the states. It can be assumed that greater changes in the local potential should generate states naturally much more localized at that site. Thus the necessary distance between the neighboring similar distortions for the second condition above should become shorter as the distortions become greater, further increasing the tendency for localization.

Well-localized boundary states satisfying the two conditions above should constitute flat bands inside the minimum band gap without dispersion in the reciprocal space. It is clear that the weak bond in the present $\Sigma = 3$ boundary does not completely satisfy the second condition above, because of the repetition of the cells mentioned in Sec. III D. Thus the bands in the band gap in Fig. 11 have small dispersion. However, the present weak-bond states can be regarded approximately as localized states of the second group as discussed in Sec. III D. If the weak bonds existed more sparsely in the interface, the generated states should become well localized in directions parallel to the interface.

The second condition above is also not satisfied for the shallow band-edge states observed in the $\langle 111 \rangle$ $\Sigma = 7$ and $\langle 011 \rangle$ $\Sigma = 3$ twist boundaries. The degree of bond distortion is large enough to generate the states inside the minimum band gap, and thus these states are well localized within the interface layers. However, similar bond distortions exist with a high density in these twist boundaries. Thus these boundary-localized states are not localized in directions parallel to the interface, as shown in Sec. III. In these cases, the smaller degree of bond distortions compared to weak bonds makes it more difficult to satisfy the second condition mentioned above.

Neither of the two conditions above is satisfied for boundary-localized states of the CSL tilt boundaries such as the $\{122\}$ $\Sigma = 9$ boundary. The bond distortions are relatively small, which results in no states inside the minimum band gap. Further, the bond distortions or structural disorder are arranged in the interface with short periods, particularly along the rotation axis. Thus the boundary states are not localized in directions parallel to the interface.

The present argument about the two conditions for the well-localized boundary states should also apply to interfaces without any two-dimensional periodicity, such as boundaries with infinitely large CSL unit cells. In such cases, band-edge states caused by bond distortions should not be so localized in directions parallel to the interface when similar bond distortions exist with a high density, as we saw in the $\langle 111 \rangle$ $\Sigma = 7$ and $\langle 011 \rangle$ $\Sigma = 3$ boundaries in Secs. III B and III C. This is because such states propagate along the interface through such neighboring similar distorted sites, in spite of the lack of periodicity. Of course, it should be possible for even relatively small bond distortions to generate well-localized states of the second group when similar bond distortions are distributed sparsely.

On the other hand, from another point of view, the boundary-localized states of the first group can be regarded as peculiar electronic states of interface layers with peculiar atomic configurations between the two bulk crystals, especially in the cases of CSL boundaries with two-dimensional periodicity. This point can be understood by considering the quantum well of a superlattice where a thin semiconductor layer is sandwiched by the other kind of semiconductor with a different bandwidth. In such a case, when electronic states of the central semiconductor layer for a given two-dimensional k vector exist in the forbidden energy regions of the projected band structure of the bulk semiconductors on both sides for the same two-dimensional k vector, they cannot be propagated into the bulk semiconductors on both sides. Thus these states are localized in the central layer. However, these states are not localized in directions parallel to the interface, but propagate along the layer. This argument does not require the electronic states localized in the central layer to exist inside the minimum band gap of the bulk semiconductors on both sides, but only requires that such states exist in the forbidden energy regions in the projected two-dimensional band structure of the bulk semiconductors on both sides, such as pseudogaps in the bands, regions inside the band gap below the valence-band maximum or above the conduction-band minimum, or regions below the valence band. This argument explains well the boundary-localized states of the CSL tilt boundaries, such as the $\{122\}$ $\Sigma = 9$ boundary in particular.

About the localized band-edge states in amorphous Si, it can be said that there exist two kinds of localized states. The first kind are bulklike states at band edges localized to bulklike regions surrounded by distorted regions, as pointed out by Cohen et al.[36] and Singh[37] and mentioned in Sec. IV B. These localized states are caused by the suppression of bulklike states at the band edges by the structural disorder, such as odd-membered rings and dihedral-angle disorder. The energy levels of these states should not penetrate into the minimum band gap, but should exist within the bands between the bulk band edge and the mobility edge. The second kind of states are those localized to distorted regions because of a local electronic structure peculiar to distorted regions, as discussed by Ching and Lin.[42] States of this kind should constitute band tails penetrating into the minimum band gap in amorphous Si. These states have been found in linear combination of atomic orbitals (LCAO) (Ref. 42) and tight-binding[43] supercell calculations of fourfold-coordinated models of amorphous Si.

The present boundary-localized states are similar to the second kind of localized states in amorphous Si. The first kind of localized states in amorphous Si cannot be localized at grain boundaries in Si with the bulk crystals on both sides, because the width of interface regions is not sufficiently large in general. It seems that the present boundary-localized states of the two groups discussed above correspond to the weak and strong localization within the second kind of localized states in amorphous Si.[42,43]

Finally, comparing states at the top of the valence band and those at the bottom of the conduction band, stronger localization behavior has been observed for the conduction-band-edge states rather than the valence-band-edge states in calculations of amorphous Si.[42,43] Similarly, there exists a tendency for boundary-localized states to be generated more frequently at the conduction-band edge rather than at the valence-band edge, as discussed in Sec. IV A. Regarding the localization behavior in directions parallel to the interface, it is greater in the upper weak-bond states rather than in the lower weak-bond states as shown in Sec. III D. However, we find no clear differences in this point between the generated shallow band-edge states at the valence-band and conduction-band edges.

D. Origins of the observed band tails at grain boundaries in Si

Various experiments[19-22] have shown the presence of exponential band tails at grain boundaries in polycrystalline Si or in Si bicrystals. These band tails penetrate into the minimum band gap, and have features similar to those observed in amorphous Si or in Si/SiO$_2$ interfaces.[21] It seems that such band tails are intrinsic properties of grain boundaries in Si, as are the band tails in amorphous Si, although many experiments have indicated that deep levels are frequently generated extrinsically by impurities such as transition metals or oxygen.[2,21,23,25]

The present structural disorder generating shallow gap states, namely bond distortions such as bond stretchings and bond-angle distortions, and greatly stretched bonds, are candidates for the origins of the experimentally observed band tails at grain boundaries in Si. The present twist boundaries themselves do not necessarily exist stably in real polycrystalline Si as compared with the stable CSL tilt boundaries as discussed in paper I. But the present configurations of our twist boundaries can be regarded as models of local structures of general grain boundaries or defects in the CSL tilt boundaries such as steps, facet junctions, intersections, or dislocations. Thus distorted or weak bonds similar to the present ones should exist in such regions, which should cause shallow band edges states or well-localized deeper weak-bond states as seen in the present calculations. The degree of distortions and the spatial distribution of such distorted or weak bonds, which should be controlled by the energetics, should determine the depth in the band gap and the degree of localization of the generated states as discussed above. In this way, the observed band tails must be generated.

It should be noted that previous calculations showed only that the CSL tilt boundaries contain no states inside the minimum band gap. Also, no calculations of grain boundaries in Si successfully explained the origins of the band tails. The present calculations have shown that structural disorder (with the exception of coordination defects) in grain boundaries in Si can indeed generate electronic states penetrating into the minimum band gap consistent with the observed band tails. In particular, the present weak-bond states, which are relatively deep in the band gap and exhibit relatively strong localization, are a typical realistic model for the origin of the band tails. It can be said that the present study has settled the long-standing discrepancy[2,21,31] between theoretical calculations and experiments about the band tails at grain boundaries in Si.

It should be noted that odd-membered rings and dihedral-angle disorder are not so important as the origins of the band tails at grain boundaries in Si. This point is in contrast to previous arguments about the band tails in amorphous Si. This is because the effects of odd-membered rings and dihedral-angle disorder on the band edges are concerned mainly with the localization to bulk-like regions, as discussed above.

The present view is consistent with recent experiments indicating the intrinsic origins of the band tails in polycrystalline Si. Jousse, Delage, and Iyer[22] found that the densities of shallow states at grain boundaries in polycrystalline Si films are substantially decreased by a hydrogen-plasma treatment, as well as the densities of deep levels, which greatly steepens the band tails. This phenomena can be explained by the replacement of distorted or weak Si-Si bonds by Si-H bonds, which is consistent with the absorbed hydrogen concentration. Yasutake et al.[23] have shown that the densities of gap states at grain boundaries in Si containing a low concentration of impurities but generated by rapid solidification are substantially decreased by the annealing in Ar. This indicates that high densities of distorted or weak bonds as well as coordination defects generating shallow or deep states are contained in grain boundaries generated by rapid solidification, and that these are decreased or relaxed by the annealing in Ar.

V. CONCLUSION

By examining the atomic and electronic structures of the tilt and twist boundaries in Si, relations between the structural disorder and local electronic structure have been clarified. Various kinds of structural disorder, such as odd-membered rings, bond distortions (bond stretchings and bond-angle distortions), four-membered rings containing large bond-angle distortions, weak bonds, and dihedral-angle distortions, have been shown to have characteristic effects on the local electronic structure of Si. These effects are essentially consistent with those obtained by previous theoretical studies of amorphous Si. However, the present study has shown the effects of the respective kinds of structural disorder much more clearly than previous studies of amorphous Si, because the respective kinds of disorder can be arranged and buried properly between the bulk crystals in the configurations of grain boundaries.

It has been shown that bond distortions at grain boundaries generate electronic states at the band edges. These band-edge states are frequently localized in the interface layers, although these states are not necessarily localized in the directions parallel to the interface. Greater bond distortions existing isolated or sparsely in the interface can generate states deeper in the band gap with stronger localization behavior in directions parallel to the inter-

face, as in the case of the present weak-bond states.

The reason why the CSL tilt boundaries in Si or Ge contain no electronic states inside the minimum band gap is that the degree of bond distortions is not so great in accordance with the small interfacial energies of such boundaries. In the present study, we have shown examples of grain boundaries in Si with no coordination defects but with bond distortions sufficient to generate states inside the minimum band gap. The configurations of such boundaries can be regarded as models of local structures of general grain boundaries or defects in the observed CSL tilt boundaries in Si. Thus the present kinds of distorted or weak bonds should be regarded as the origins of the experimentally observed band tails at grain boundaries in Si. The present study has settled the long-standing discrepancy between theoretical studies and experiments about the band tails at grain boundaries in Si.

ACKNOWLEDGMENTS

[1] See papers in *Polycrystalline Semiconductors*, edited by H. J. Möller, H. P. Strunk, and J. H. Werner, Springer Proceedings in Physics Vol. 35 (Springer, Berlin, 1989); *Polycrystalline Semiconductors II*, edited by J. H. Werner and H. P. Strunk, Springer Proceedings in Physics Vol. 54 (Springer, Berlin, 1991); *Polycrystalline Semiconductors III*, edited by H. P. Strunk, J. H. Werner, B. Fortin, and B. Bonnaud (Trans Tech, Switzerland, 1994).

[2] J. Thibault, J. L. Rouviere, and A. Bourret, in *Materials Science and Technology*, edited by R. W. Cahn, P. Haasen, and E. J. Kramer (VCH, Weinheim, 1991), Vol. 4, p. 321.

[3] A. Garg, W. A. T. Clark, and J. P. Hirth, Philos. Mag. A **59**, 479 (1989).

[4] O. L. Krivanek, S. Isoda, and K. Kobayashi, Philos. Mag. **36**, 931 (1977).

[5] M. D. Vaudin, B. Cunningham, and D. G. Ast, Scripta Metall. **17**, 191 (1983).

[6] A. Bourret and J. J. Bacmann, Surf. Sci. **162**, 495 (1985); Trans. Jpn. Inst. Met. Suppl. **27**, 125 (1986).

[7] J. Thibault-Desseaux and J. L. Putaux, in *Structure and Properties of Dislocations in Semiconductors 1989*, edited by S. G. Roberts, D. G. Holt, and P. R. Wilshaw, IOP Conf. Series No. 104 (Institute of Physics, Bristol, 1989), p. 1.

[8] A. Bourret and J. L. Rouviere, in *Polycrystalline Semiconductors* (Ref. 1), p. 8.

[9] Y. Ishida and H. Ichinose, in *Polycrystalline Semiconductors* (Ref. 1), p. 42.

[10] R. E. Thomson and D. J. Chadi, Phys. Rev. B **29**, 889 (1984).

[11] D. P. DiVicenzo, O. L. Alerhand, M. Schlüter, and J. W. Wilkins, Phys. Rev. Lett. **56**, 1925 (1986).

[12] A. Mauger, J. C. Bourgoin, G. Allan, M. Lannoo, A. Bourret, and L. Billard, Phys. Rev. B **35**, 1267 (1987).

[13] A. T. Paxton and A. P. Sutton, J. Phys. C **21**, L481 (1988); Acta Metall. **37**, 1693 (1989).

[14] M. Kohyama, R. Yamamoto, Y. Ebata, and M. Kinoshita, J. Phys. C **21**, 3205 (1988).

[15] M. Kohyama, R. Yamamoto, Y. Watanabe, Y. Ebata, and M. Kinoshita, J. Phys. C **21**, L695 (1988).

[16] M. Kohyama, S. Kose, M. Kinoshita, and R. Yamamoto, J. Phys. Condens. Matter **2**, 7809 (1990).

[17] A. V. Nikolaeva, A. V. Artemyev, Yu. H. Vekilov, L. K. Fionova, and M. B. Samsonova, J. Phys. Condens. Matter **4**, 2775 (1992).

[18] T. A. Arias and J. D. Joannopoulos, Phys. Rev. Lett. **69**, 3330 (1992); Phys. Rev. B **49**, 4525 (1994).

[19] J. Werner and M. Peisl, Phys. Rev. B **31**, 6881 (1985).

[20] A. J. Madenach and J. H. Werner, Phys. Rev. B **38**, 13 150 (1988).

[21] J. H. Werner, in *Structure and Properties of Dislocations in Semiconductors 1989* (Ref. 7), p. 63.

[22] D. Jousse, S. L. Delage, and S. S. Iyer, Philos. Mag. B **63**, 443 (1991).

[23] K. Yasutake, A. Takeuchi, K. Yoshii, H. Kawabe, J. Masuda, and K. Kaneko, in *Technical Digest of the 5th International Photovoltaic Science and Engineering Conference, Kyoto, Japan, 1990* (Publication Office of the International PVSEC-5, Kyota Univ., 1990), p. 307.

[24] M. Kohyama, S. Kose, M. Kinoshita, and R. Yamamoto, J. Phys. Condens. Matter **1**, 8251 (1989).

[25] J.-L. Maurice, in *Polycrystalline Semiconductors II* (Ref. 1), p. 166; Philos. Mag. A **68**, 957 (1993).

[26] M. Kohyama and R. Yamamoto, Phys. Rev. B **49**, 17 102 (1994).

[27] S. Sawada, Vacuum **41**, 612 (1990).

[28] M. Kohyama, J. Phys. Condens. Matter **3**, 2193 (1991).

[29] E. Tarnow, P. Dallot, P. D. Bristowe, J. D. Joannopoulos, G. P. Francis, and M. C. Payne, Phys. Rev. B **42**, 3644 (1990); E. Tarnow, T. Arias, P. D. Bristowe, P. Dallot, G. P. Francis, J. D. Joannopoulos, and M. C. Payne, in *Atomic Scale Calculations of Structure in Materials*, edited by M. S. Daw and M. A. Schlüter, MRS Symposia Proceedings No. 193 (Materials Research Society, Pittsburgh, 1990), p. 235.

[30] Preliminary accounts have been given in M. Kohyama, S. Kose, and R. Yamamoto, in *Defect Engineering in Semiconductor Growth, Processing and Device Technology*, edited by S. Ashok, J. Chevallier, K. Sumino, and E. Weber, MRS Symposia Proceedings No. 262 (Materials Research Society, Pittsburgh, 1992), p. 567; M. Kohyama and R. Yamamoto, in *Amorphous Silicon Technology—1993*, edited by E. A. Schiff, M. J. Thompson, A. Madan, K. Tanaka, and P. G. LeComber, MRS Symposia Proceedings No. 297 (Materials Research Society, Pittsburgh, 1993), p. 177; M. Kohyama and R. Yamamoto, in *Polycrystalline Semiconductors III* (Ref. 1), p. 55.

[31] A. P. Sutton, in *Structure and Properties of Dislocations in Semiconductors 1989* (Ref. 7), p. 13.

[32] J. D. Joannopoulos and M. L. Cohen, Phys. Rev. B **7**, 2644 (1973).

[33] K. Winer and S. K. Bose, Phys. Rev. B **38**, 12 683 (1988).

[34] J. D. Joannopoulos, Phys. Rev. B **16**, 2764 (1977); J. D. Joannopoulos and D. C. Allan, in *Advances in Solid State Physics*, edited by J. Treusch (Vieweg, Braunschweig, 1981), Vol. 21, p. 167.

[35] B. K. Agrawal, S. Agrawal, P. S. Yadav, and J. S. Negi, J.

Phys. Condens. Matter **2**, 6519 (1990).

[36]M. H. Cohen, H. Fritzsche, J. Singh, and F. Yonezawa, J. Phys. Soc. Jpn. **49**, 1175 (1980).

[37]J. Singh, Phys. Rev. B **23**, 4156 (1981).

[38]R. Biswas, C. Z. Wang, C. T. Chan, K. M. Ho, and C. M. Soukoulis, Phys. Rev. Lett. **63**, 1491 (1989).

[39]S. K. Bose, K. Winer, and O. K. Andersen, Phys. Rev. B **37**, 6262 (1988).

[40]I. Stich, R. Car, and M. Parrinello, Phys. Rev. B **44**, 11 092 (1991).

[41]P. A. Fedders, D. A. Drabold, and S. Klemm, Phys. Rev. B **45**, 4048 (1992).

[42]W. Y. Ching and C. C. Lin, Phys. Rev. B **18**, 6829 (1978).

[43]C. S. Nichols and K. Winer, Phys. Rev. B **38**, 9850 (1988).

[44]D. J. Chadi, Phys. Rev. Lett. **41**, 1062 (1978); Phys. Rev. B **29**, 785 (1984); A. T. Paxton, A. P. Sutton, and C. M. M. Nex, J. Phys. C **20**, L263 (1987).

[45]D. Tomanek and M. A. Schlüter, Phys. Rev. Lett. **56**, 1055 (1986); Phys. Rev. B **36**, 1208 (1987).

[46]H. J. Monkhorst and J. D. Pack, Phys. Rev. B **13**, 5188 (1976).

[47]C. R. M. Grovenor, J. Phys. C **18**, 4079 (1985).

[48]L. Ley, S. Kowalczyk, R. Pollack, and D. A. Shirley, Phys. Rev. Lett. **29**, 1088 (1972).